1968

Flow through a converging-diverging tube and its implications in occlusive vascular disease

John Harold Forrester
Iowa State University

69-9857

FORRESTER, John Harold, 1939-

FLOW THROUGH A CONVERGING-DIVERGING TUBE AND ITS IMPLICATIONS IN OCCLUSIVE VASCULAR DISEASE.

Iowa State University, Ph.D., 1968

Engineering Mechanics

University Microfilms, Inc., Ann Arbor, Michigan

FLOW THROUGH A CONVERGING-DIVERGING TUBE AND ITS IMPLICATIONS IN OCCLUSIVE VASCULAR DISEASE

by

John Harold Forrester

A Dissertation Submitted to the
Graduate Faculty in Partial Fulfillment of
The Requirements for the Degree of
DOCTOR OF PHILOSOPHY

Major Subject: Engineering Mechanics

Approved:

Signature was redacted for privacy.

In Charge of Major Work

Signature was redacted for privacy.

Head of Major Department

Signature was redacted for privacy.

Dean of Graduate College

Iowa State University
Ames, Iowa

1968

TABLE OF CONTENTS

I. INTRODUCTION

A. Incentive for Studying Problem

A major incentive for studying the flow of an incompressible fluid through a converging-diverging tube comes from the medical field. In the arterial systems of mammals, it is quite common to find narrowings, or stenoses, some of which are, at least approximately, axisymmetric or "collar-like". These constrictions may be caused by intravascular plaques or the impingement of ligaments or spurs on the vessel wall (1,2). Once a vascular lesion has developed, there may be a "coupling" effect between its further development and the changed flow characteristics (3). A knowledge of the flow characteristics in the vicinity of a stenosis may help to further understand some of the major complications which can arise from such constrictions. These include:

(a) An ingrowth of tissue into the artery

(b) The development of a thrombus (an intravascular clot)

(c) The weakening and bulging of the artery downstream from the stenosis (post-stenotic dilatation).

An ingrowth of tissue into the artery not only causes an increased resistance to flow, but it may also reduce the blood flow through the artery. Of course the tissue may continue to grow until the artery is completely occluded.

The formation of mural thrombi at the location of a narrowed artery results in the same complications as for the ingrowth of tissue. There is the additional hazard of a piece breaking off (an embolus) and subsequently lodging in a smaller vessel, thus blocking the flow. The weakening and subsequent bulging of the artery downstream from a stenosis introduces the possibility of rupture with fatal consequences.

Until recently, it has commonly been thought that atherosclerotic plaques are caused primarily by faulty lipid metabolism. Since these plaques are rich in lipids and are quite often found in animals which have been fed a high cholesterol diet, most of the research on the causes of atheroma has been concerned with the metabolism of lipids. However, Fox and Hugh (4) suggest another possible cause of atherosclerosis. It is their proposal that the development of atheroma is due to intravascular clotting. They credit Rokitansky (5) with originating the idea in 1844, and argue that since atherosclerotic lesions are most commonly found at the entrances of branching vessels, in curved arterial segments, or generally at locations of abrupt changes in geometry (and thus in the flow characteristics), that any theory for their formation and growth must take into account the flow characteristics of the blood. Fox and Hugh (4) indicate that in the arterial system static zones occur, which are due to separation of the main flow from the walls of the

arteries. It is suggested that in these zones there is an interaction of platelets and fibrin to form a mesh in which lipid particles become trapped, with the subsequent formation of a plaque of atheroma. Certainly thrombus formation is one of the major complications of prosthetic heart valves, and many investigators have suggested that stagnation zones near the valve contribute to the formation of thrombi. Thus it seems reasonable that if separation regions of relatively stagnant flow occur near stenoses, that they may well contribute to the problems of thrombosis.

A primary goal of the present investigation was to predict analytically when (at what Reynolds number) and where (along the stenosis) separation of the flow occurs for a stenosis of given geometry. An experimental program was carried out to check the theory. In the theoretical development the fluid is assumed to be Newtonian. Thus it might be reasonably valid for water or glycerol-water solutions (which are commonly used as blood analogs) but not necessarily valid for whole blood, which behaves as a non-Newtonian fluid under certain flow conditions. Therefore, in addition to water and glycerol-water solutions, whole blood was also used in the system, and the results obtained (pressure drop and the region of separation) are compared with the other experimental results as well as with those predicted theoretically. The author is not aware of any similar investigations

in which the flow characteristics of blood are compared to those of a blood analog.

In the medical literature on atherosclerosis and its attendant complications of thrombosis and aneurysm formation, one can find other flow characteristics mentioned which are believed to contribute to the formation and growth of vascular lesions. Such terms as pressure, shearing stress, vortices, and turbulence, are frequently mentioned (see for example references 1-9). Some of these ideas will be considered when discussing the theoretical and experimental results.

Finally, it should not be concluded that the flow characteristics of blood are the only factors to consider in the development of vascular lesions. Certainly the rheological properties of the tissues (blood and arterial wall), the electro-chemical environment near the arterial wall, and the biochemistry and histology of the tissues must be studied in conjunction with the flow characteristics in hopes of obtaining a better understanding of arterial disease.

B. Statement of Problem

The specific problem which is considered, both theoretically and experimentally, in this investigation is that of the steady, laminar, axisymmetric flow of an incompressible fluid through a rigid converging-diverging tube. As noted previously for the theoretical analysis, the fluid is

considered to be Newtonian. The walls of the tube are taken to be straight and parallel except in the converging-diverging portion. Since only axisymmetric flow is considered, the tube must have circular cross sections at all locations. A sketch of the tube together with the forms of velocity profiles which are intuitively expected at various sections, is shown in Fig. 1.

It is noted in Fig. 1 that in the diverging portion of the tube a region is shown where the fluid adjacent to the walls is moving in a direction opposite to that of the main stream. The fluid inside the region bounded by the dotted lines is expected to circulate in the manner indicated, and not move downstream with the main body of fluid. The dotted lines represent a streamline (a line which is everywhere tangent to the velocity vectors) and the phenomenon indicated is known as streamline separation, or simply separation. The separation point and the reattachment point are located at the upstream and downstream ends, respectively, of the separation region. Due to symmetry these points form a continuous curve circumferentially around the tube so that there actually exists "separation and reattachment lines". Streamline separation will be discussed further in Sec. C of this chapter.

An approximate solution which predicts the velocity profiles along the converging-diverging tube has been obtained

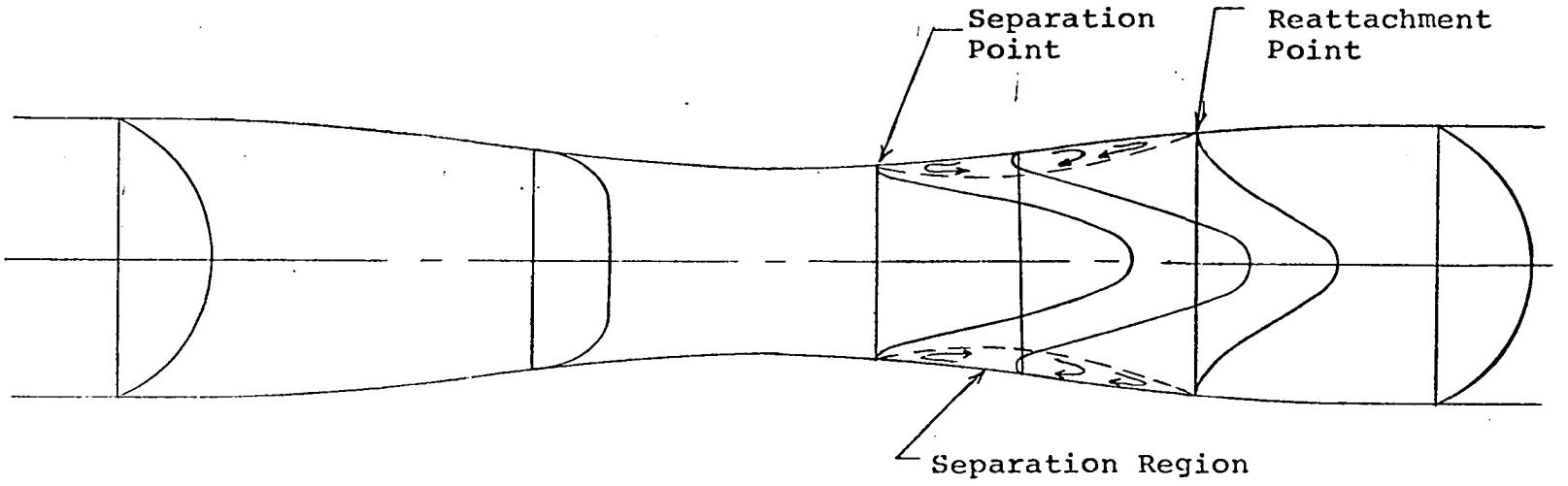

Figure 1. Expected velocity profiles in a converging-diverging tube

and is described in Chapter III. Expressions are also obtained for the separation and reattachment points (if separation occurs), the wall shearing stress, and the pressure drop along the stenosis.

Admittedly, some of the restrictions imposed upon the problem are not satisfied in a biological system. Therefore, each of the assumptions will be considered in more detail in the following paragraphs.

The first assumption listed is that of steady flow; this assumption is definitely not valid in the larger arteries. McDonald (10) states that if the parameter $R_o (\omega/\nu)^{\frac{1}{2}}$ is less than one, then the flow may be treated as quasi-steady, where R_o is the radius of the artery, ω is the characteristic frequency of the pulsations, and ν is the kinematic viscosity of the blood. This condition is usually satisfied in the smaller arteries. There may also be cases where a quasi-steady flow is obtained in some of the larger arteries, due to a congenital or acquired constriction in a major artery (11). Bernstein, et al. (12) state that a minimal pulsatile flow is obtained as the result of coarctation of the aorta, "pulseless disease", arteriosclerotic occlusions of various major arterial branches, and severe aortic stenosis. Therefore, it must be concluded that the restriction of steady flow is a severe one, but that it may be a reasonably good assumption in certain parts of the arterial system.

The assumption of laminar flow is not expected to be restrictive in those portions of the arterial system where the flow is nearly steady. A "collar-like" stenosis (centrally located between any two branches) in a relatively straight artery will fit the ideal geometry about as well as can be expected. This type of configuration will approximate the axisymmetric condition.

Blood may be considered to be an incompressible fluid, but the assumption of a rigid tube should be discussed. An artery is a slightly tapered tube which has viscoelastic properties. However, neither one of these characteristics is expected to seriously affect the results obtained for steady flow. If a stenosis has developed, the arterial wall has undoubtedly undergone some complex physiological changes, but the gross result is generally a hardening of the walls of the artery. The slight taper of the arterial walls in the direction of flow will tend to stabilize the flow which is entering and leaving the converging-diverging section. If the arterial wall upstream and downstream is not extremely smooth, any taper which helps to stabilize the flow will be an asset.

Although blood is actually a non-Newtonian suspension of cells in plasma, it may be considered to flow as a homogeneous, Newtonian fluid in vessels greater than 0.5 mm in diameter (10). Other investigators (13, 14, 15) have found

that the rheological characteristics of blood arise from the action of fibrinogen on the red blood cells, and that blood does have a yield stress (due to the fibrinogen). They have concluded that the non-Newtonian characteristics of blood are apparent only at low rates of shear, and that for shear rates above 100 sec^{-1}, blood can be considered to be a Newtonian fluid. Thus it was expected that the non-Newtonian characteristics of blood would not be important in the present investigation, except possibly in the vicinity of the separation region where low shear rates would occur.

C. Streamline Separation

"Poiseuille flow" is obtained for the case of fully developed, steady laminar flow of a viscous, incompressible, Newtonian fluid flowing through a straight circular tube. The velocity profile is parabolic at any section along the tube, the streamlines are straight and parallel, and there is no change in any of the flow characteristics along the tube. If a converging-diverging section is added, the velocity profiles will change, and thus cause a change in the other flow characteristics.

When streamlines are converging in the direction of flow, the negative pressure gradient associated with the convective acceleration (the mean velocity increases in the direction of flow) combines with the viscous effects in retarding the

fluid elements. Thus, in a slightly converging tube, the velocity distribution near the center of the tube becomes somewhat flatter than the parabolic distribution, and the slight convergence has a tendency to stabilize the laminar mode of flow (16).

When the streamlines are diverging, the mean velocity decreases in the direction of flow and there is an increase in pressure due to the Bernoulli effect. This increased pressure, when combined with the pressure drop due to friction, may be sufficiently large to cause an adverse pressure gradient to develop, i.e., the resultant pressure may be increasing in the direction of flow. The motion of a thin layer of fluid adjacent to the wall is retarded by the wall friction and the adverse pressure gradient, but moved forward by the fluid above it because of viscous effects. If the adverse pressure gradient becomes sufficiently large, it will cause the slowly moving particles of fluid near the wall to reverse their direction of flow and a separation region will develop. In discussing boundary layer separation, Schlichting (17) defines the separation point as the limit between the forward and reverse flow in the layer of fluid adjacent to the wall; that is where

$$\left(\frac{\partial u}{\partial y}\right)_{y=0} = 0$$

where u is the component of velocity parallel to the wall and y is in a direction normal to the wall. The same definition

may be used for the reattachment point. Because the present problem is not considered to be a boundary layer type of problem in the classical sense (no potential core of fluid is assumed), the expression "streamline separation" is preferred over the term "boundary layer separation" to describe the phenomenon. Reference to Fig. 1 indicates that the streamlines (forming a stream surface) which ran along the wall of the tube before separation occurred take new positions (dotted lines) when there is separation in the diverging portion of the tube. The separation point is a point of stagnation on the streamline which divides the oncoming flow from the reverse flow. Since there is no flow across a stream surface, the oncoming fluid must move away from the boundary at the separation point.

The pattern of flow in Fig. 1 is essentially that of laminar separation. The separation region, which is enclosed by the stream surface which passes through the separation and reattachment points, is fairly well defined, and there is no turbulent mixing within the region. As the Reynolds number is increased and the separation region grows larger, turbulent eddies will develop within the separation region, and some will move on downstream. Thus large energy losses are usually associated with separation. If the flow field preceding the constriction is turbulent, the general effect is to delay separation by either moving the separation point

downstream, or to maintain flow without separation (18). This is due to the mixing action of turbulence which tends to replace the normally slow moving fluid near the boundary with fluid of higher kinetic energy.

To conclude this section, some general characteristics of the separation phenomenon which make it difficult to predict analytically will be mentioned. For a more complete discussion, references 16-21 should be consulted.

It was noted that separation is caused by an adverse pressure gradient. Once separation does occur, the pressure distribution is modified, and the separation point moves upstream to an equilibrium position. Further, adverse pressure gradients favor the transition to turbulent flow, so the flow may be expected to become turbulent at lower Reynolds numbers than are required in straight pipe flow. The flow in a diverging geometry is inherently unstable, and non-symmetrical velocity distributions may be expected. Random variations in pressure and velocity within a separation region may be expected except at small Reynolds numbers which are slightly above the critical Reynolds number required to cause separation.

Because of the characteristics of the separation phenomena mentioned above, it is very difficult to characterize separation phenomena.

II. REVIEW OF LITERATURE

A. Theoretical Work

1. General review

Ideally, the motion of an incompressible, Newtonian fluid through a tube of axially varying cross section can be described exactly by the Navier-Stokes equations of motion and the equation of conservation of mass. However, to the author's knowledge, the problem has not been studied extensively because of the inability to solve the resulting non-linear equations together with their associated boundary conditions. In reviewing the literature on flow through tubes or channels having non-parallel walls one is continually referred back to the work of Blasius (22), Jeffery, (23) and Hamel (24).

Blasius investigated in 1910 the cases of two dimensional and axisymmetric steady flow through channels and tubes with small exponential divergence. Using a method of successive approximations, he developed a solution of the two-dimensional Navier-Stokes equations. He found that backflow will occur in a divergent channel when $mRe = \frac{35}{2}$, where m is the slope of the channel and Re is the Reynolds number.

Blasius also briefly outlined how the same type of procedure could be used to calculate the flow patterns in a slightly diverging (exponentially) tube of circular cross section. Since the theoretical results of the author's in-

vestigation are similar to those obtained by Blasius for the diverging tube, a more detailed review of his work will be given in a separate section of this chapter.

Abramowitz (25) extended the Blasius theory for linearly diverging channels and, for a fixed mRe, has shown that the separation point moves downstream from the entrance as the Reynolds number is increased and the angle of divergence is decreased.

The case of two-dimensional, steady flow in a wedge-shaped convergent or divergent channel was studied by Jeffery (23) in 1915 and independently by Hamel (24) in 1916 (17). Using the assumptions that the entrant flow was radial, exact solutions to the Navier-Stokes equations in polar coordinates were obtained in the form of elliptic functions.

It was hoped that an analog of the Jeffery-Hamel solutions could be found for the axisymmetric problem of source flow from the apex of a cone. If such a solution existed, it could possibly be extended for flow through a converging-diverging tube. However, Langlois (26) states that researchers have been unsuccessful in trying to find an exact solution to the axisymmetric problem. He shows for the cone problem that one cannot make the assumption of purely radial flow, at least for an incompressible fluid without body forces. There must also be a velocity component in the θ - direction (measured from the axis of the cone), so that eddies are

formed. Thus he concludes there is little hope of obtaining an exact solution for this flow problem, as the Navier-Stokes equations are too complicated.

The problem of steady flow through an axially symmetric, time-dependent stenosis in a rigid tube was studied by Young (3). As in the present investigation, his incentive for studying the problem came from the biological area, and he discussed some possible biological reactions of the flow. As a growth in an artery becomes larger, one expects that the flow characteristics will change. Thus Young classified a developing stenosis into three stages. The first stage includes the initial development of the stenosis. The size of the protuberance is considered to be small enough so that no flow separation occurs. As the lesion continues to develop and project into the lumen, a geometry is obtained such that separation occurs and laminar backflow develops. Thus a second stage (Stage II) is reached. Stage III occurs when the stenosis has grown to such a size that turbulence develops in the separated region, and the region is no longer localized but extends downstream.

In his analysis, Young considered flow through a "mild" stenosis (Stage I). By performing an order of magnitude analysis, he showed that the Navier-Stokes equations and continuity equation reduced to the two equations obtained for Poiseuille flow, i.e. the convective acceleration terms

were negligible. Thus a parabolic velocity distribution was obtained at each cross section, and the local pressure gradient and wall shearing stress relationships at any given position along the stenosis were the same as those for Poiseuille flow through a tube having the same diameter as the given cross section. From Young's plots, it is observed that the pressure drop across the stenosis and the wall shearing stress at the throat increase rapidly as the height of the growth is increased.

2. Summary of Blasius' solution

Reference has already been made to the work of Blasius (22). The purpose here is to briefly summarize the method he used to study the flow characteristics in a slightly diverging tube of circular cross sections. The notation used will be the same as that used in Chapter III.

Blasius restricted his investigation to tubes where R (the radius) varied slowly with z, (the axial coordinate), and stated that every differentiation with respect to z should lower the order of magnitude, e.g. $R = a + be^{\varepsilon z}$ where ε is a small quantity. He argued that since $\frac{dR}{dz}$ was small, v (the radial component of velocity) would remain small like ε, and, in general, every differentiation with respect to z, even of u (the axial component of velocity) and v, would cause a decrease in the order of magnitude. As in the present investigation, he started with the Navier-Stokes equations for

axisymmetric flow, and used a method of successive approximations in conjunction with an order-of-magnitude analysis to obtain his results.

In his first approximation, Blasius assumed (by means of an order-of-magnitude analysis) that a parabolic velocity distribution existed at each cross section of the tube. He found that

$$u_1 = \frac{2Q}{\pi R^2}\left[1 - \frac{r^2}{R^2}\right] = 2\bar{U}\left[1 - \frac{r^2}{R^2}\right]$$

$$v_1 = \frac{2Qr}{\pi R^3}\frac{dR}{dz}\left[1 - \frac{r^2}{R^2}\right] = 2\bar{U}\frac{r}{R}\left[1 - \frac{r^2}{R^2}\right]\frac{dR}{dz}$$

$$\frac{\partial p_1}{\partial z} = -\frac{8\mu Q}{\pi R^4}$$

where Q is the volumetric flow rate, $\bar{U}$ is the average velocity at any cross section, μ is the absolute viscosity of the fluid, and p is the static pressure. The subscript 1 refers to the first approximation. It is noted that v_1 is of the order of εu_1.

For his second approximation, Blasius substituted

$$u = u_1 + u_2$$

$$v = v_1 + v_2$$

$$p = p_1 + p_2$$

into the original three equations and again looked at the order-of-magnitude of the terms involved. The terms in u_1, v_1, and p_1 that didn't go to zero because of the first

approximation became the impressed forces (the inertia terms) of the second approximation. Thus Blasius' method amounts to calculating the inertia terms from the first approximation and introducing them into the equations as external forces for the second approximation. This procedure is commonly used to extend the equations of creeping motion to applications involving larger Reynolds numbers. However, the method gets extremely long and difficult after two approximations, and Blasius stated that there was no need to go further. The results he obtained are as follows:

$$\frac{\partial p}{\partial z} = \frac{\partial p_1}{\partial z} + \frac{\partial p_2}{\partial z} = -\frac{8\mu Q}{\pi R^4} + \frac{4\rho Q^2}{\pi^2 R^5}\frac{dR}{dz}$$

$$u = u_1 + u_2 = \frac{2Q}{\pi R^2}\left[1 - \frac{r^2}{R^2}\right] + \frac{4Q^2}{\pi^2 \nu}\frac{1}{R^3}\frac{dR}{dz}\left[\frac{1}{18} - \frac{1}{4}\frac{r^2}{R^2} + \frac{1}{4}\frac{r^4}{R^4} - \frac{1}{18}\frac{r^6}{R^6}\right]$$

Blasius specified the condition for separation as

$$\left.\frac{\partial u}{\partial r}\right|_{r=R} = 0$$

or

$$\frac{Q}{\nu R}\frac{dR}{dz} = 6\pi$$

where ν is the kinematic viscosity of the fluid.

These results will be compared with those obtained in the present investigation in Chapter III.

B. Experimental Work

An attempt was made to uncover experimental data on the velocity profile and/or pressure distribution for an incompressible, Newtonian fluid flowing through a converging-diverging tube. Only one applicable study was found. In an experimental investigation using air flowing through an exponentially diverging two-dimensional channel, Patterson (27) measured the velocity profiles along the channel and compared his results to those predicted by Blasius. Using a Reynolds number of 35, (based on throat conditions) Patterson found (for the channel he had constructed) that the experimental and theoretical profiles superimposed up to the value of $Re \frac{dz}{dx} = 2$ where z is the wall coordinate and x is the axial coordinate. Since the wall slope must be small to satisfy the Blasius theory, this value seems reasonable for a Reynolds number of 35. However, even for values of $Re \frac{dz}{dx}$ up to 8.70 (the largest investigated by Patterson) there is less than 15% maximum deviation between the velocity profiles as measured by Patterson (see p. 683 of reference) and as predicted using the Blasius theory. Separation (which was symmetrical) was observed to commence at $Re \frac{dz}{dx} = 6.00$ as compared to the value of 17.5 which is predicted from the Blasius theory. Since Patterson was using a Reynolds number of 35, the wall slope $\frac{dz}{dx}$ was equal to 0.171 (6.00/35), which may be too large to satisfy Blasius'

requirement that the slope be small. Patterson had found in earlier work (28) that for his channel the velocity profiles were only symmetrical up to Re = 36, and thus his reason for choosing a Reynolds number of 35.

Many medical researchers have attempted to correlate the formation and growth of vascular lesions with the hydrodynamics of blood flow. Of particular interest to the present investigation are those studies which have been made to determine the effects of external constriction of arteries in experimental animals. Three studies involving three different aspects of the problem will be reviewed. To conclude this chapter, a brief discussion will be given of an investigation to quantify cellular damage associated with increased blood velocity.

Rodbard (29) has shown that progressively stenotic lesions develop in arteries of chicks and dogs which have been partially occluded by sutures. He found that in some of the animals there was an ingrowth of fibrous connective tissue into the lumen of the artery immediately distal to the suture. The geometry of the growths varied. Some ingrowths resembled those which occur in valvular stenoses while others resembled those found in coarctation of the aorta. He attributed the intimal proliferation to hydrodynamic factors which lower the pressure locally, but later (2) rejected this idea and stated that the local shear force on the vessel wall

appears to be the determinative factor.

Roach (1) states that post-stenotic dilatation can occur beyond almost every type of arterial constriction, both intrinsic and extrinsic. In a study to determine the possible cause of post-stenotic dilatation (1), he banded the femoral and/or carotid arteries in twenty-six adult dogs. He found that a "moderate" stenosis, defined by the presence of a distal thrill and bruit, always produced post-stenotic dilatation, but that none was produced by a "minimum" stenosis, defined as one with no palpable change in distal pulsation and no thrill or bruit. He concluded that a dilatation will develop if turbulence, as defined by the presence of a thrill and bruit, is present, and rejected the idea that the distension of the wall is caused by increased pressure, as proposed by some investigators.

A third complication which can arise due to the development of a stenosis is that of a reduction of flow to the vascular bed supplied by the stenosed artery. Brice, et al. (30) investigated both in vivo and in vitro the flow through and pressure drop across externally constricted human carotid arteries. They observed no significant change in either the mean flow rate or the pressure drop until the artery had been constricted so severly that the cross-sectional area was only approximately 1/6 of its original value. They attributed these phenomena to a relatively small resistance

(pressure drop/rate of flow) caused by the stenosis as compared to the total peripheral resistance. Other investigators (2, 31) have pointed out that a stenosis (excluding a very severe constriction) may not significantly affect the flow rate during resting conditions due to autoregulatory mechanisms. However, an increase in activity of the tissue supplied by the artery may well require flow rates which will be limited by the resistance of the stenosis.

Fry has made a very thorough investigation of acute endothelial changes associated with large velocity gradients (32). He inserted a plug with a narrow channel along the outer edge into the thoracic aorta of dogs. Thus the aortic blood stream was forced to rapidly converge and flow through the channel. The endothelial surface overlying the channel was therefore subjected to a large range of shearing stresses, which Fry was able to quantify. He was also able to quantify the acute changes in the endothelial histology along the channel. He found that there appeared to be an "acute yield stress", above which deterioration of the endothelial surface occurred. He also found that endothelial cells were damaged in the region of highly turbulent efflux from the plug channel, although the time-smoothed shearing stress was negligible in this region. Fry speculated that this damage was related to the turbulent energy of the efflux, and

suggested that some band of frequencies or amplitudes was required to cause the damage.

III. THEORETICAL CONSIDERATIONS

As stated in the introduction, an approximate solution will be obtained for the steady, laminar, axially-symmetric flow of an incompressible Newtonian fluid through a straight, rigid tube having in it a converging-diverging section. Only the flow field through the converging-diverging portion will be analyzed, since the geometry of the axially-varying cross section will be such that one can presume that Poiseuille flow exists upstream and downstream from the stenosis. The geometry chosen is the same as that studied by Young (3) and is shown below. The equation of the stenosis is given by the

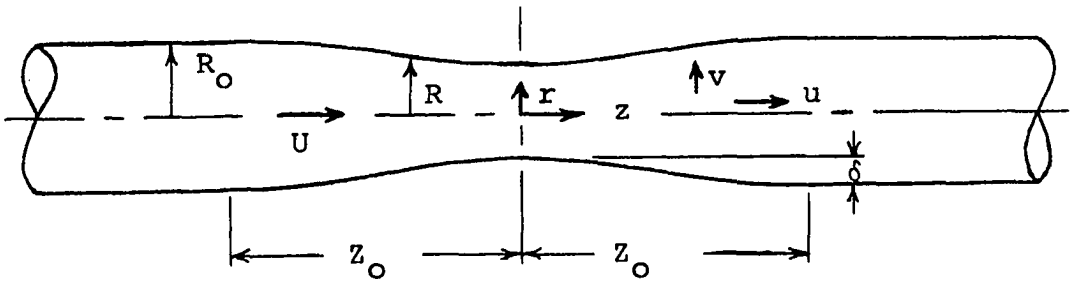

Figure 2. The converging-diverging tube

expression

$$R = R_o - \frac{\delta}{2}(1 + \cos \frac{\Pi z}{Z_o}) \qquad (1)$$

Therefore, the constriction is symmetrical about the plane $z = 0$ in addition to being axisymmetric. Cylindrical polar coordinates are used, and u and v denote the velocity components in the axial (z) direction and the radial (r) direction,

respectively. It is noted that the tube has a constant cross section except in the region $-Z_o \leq z \leq Z_o$.

If body forces are neglected, along with any motion in the circumferential direction, the Navier-Stokes equations of motion in cylindrical coordinates for steady incompressible flow reduce to

$$v\frac{\partial u}{\partial r} + u\frac{\partial u}{\partial z} + \frac{1}{\rho}\frac{\partial p}{\partial z} = \nu\left(\frac{\partial^2 u}{\partial r^2} + \frac{1}{r}\frac{\partial u}{\partial r} + \frac{\partial^2 u}{\partial z^2}\right) \tag{2}$$

$$v\frac{\partial v}{\partial r} + u\frac{\partial v}{\partial z} + \frac{1}{\rho}\frac{\partial p}{\partial r} = \nu\left(\frac{\partial^2 v}{\partial r^2} + \frac{1}{r}\frac{\partial v}{\partial r} - \frac{v}{r^2} + \frac{\partial^2 v}{\partial z^2}\right) \tag{3}$$

In Eqs. 2 and 3, the pressure gradients represent the driving forces for the flow. The non-linear convective acceleration terms account for the inertial effects of the fluid and with their inclusion the possibility of separation exists. The remaining terms in the two equations represent the viscous forces which oppose the fluid motion.

The flow field must also satisfy the continuity equation

$$\frac{\partial u}{\partial z} + \frac{1}{r}\frac{\partial}{\partial r}(rv) = 0 \tag{4}$$

Since a general solution of the above system of non-linear partial differential equations has not been obtained, it becomes necessary to work in terms of approximate models. A common approach is to perform an order-of-magnitude analysis in hopes of eliminating any terms from the equations which contribute negligibly to the problem being considered.

This method will be used in the present analysis. Dimensionless variables will be defined as follows:

$$\bar{r} = \frac{r}{R_o} \qquad \bar{z} = \frac{z}{Z_o} \qquad \bar{u} = \frac{u}{U_o}$$

$$\bar{v} = \frac{v}{U_o}\frac{Z_o}{\delta} = \frac{v}{\varepsilon U_o} \qquad \bar{p} = \frac{p}{\rho U_o^2} \qquad \bar{Re}_o = \frac{U_o R_o}{\nu} \tag{5}$$

where U_o is a characteristic velocity in the z - direction and $\varepsilon = \frac{\delta}{Z_o}$. The dimensionless space variables and the velocity components now have an order of magnitude of unity or less. Furthermore, if the functions $\bar{v}$ and $\bar{u}$ are smooth and continuous, their derivatives are also expected to have an order of magnitude of unity (33). Equations 2 to 4 are now put into dimensionless form by means of the above transformations.

$$\bar{u}\frac{\partial \bar{u}}{\partial \bar{z}} + \frac{\delta}{R_o}\bar{v}\frac{\partial \bar{u}}{\partial \bar{r}} + \frac{\partial \bar{p}}{\partial \bar{z}} = \frac{Z_o}{R_o}\frac{1}{\bar{Re}_o}\left[\frac{\partial^2 \bar{u}}{\partial \bar{r}^2} + \frac{1}{\bar{r}}\frac{\partial \bar{u}}{\partial \bar{r}} + \left(\frac{R_o}{Z_o}\right)^2 \frac{\partial^2 \bar{u}}{\partial \bar{z}^2}\right] \tag{6}$$

$$\left(\frac{\delta}{Z_o}\right)\left(\frac{R_o}{Z_o}\right)\bar{u}\frac{\partial \bar{v}}{\partial \bar{z}} + \left(\frac{\delta}{R_o}\right)^2 \bar{v}\frac{\partial \bar{v}}{\partial \bar{r}} + \frac{\partial \bar{p}}{\partial \bar{r}} =$$

$$\frac{1}{\bar{Re}_o}\left(\frac{\delta}{Z_o}\right)\left[\frac{\partial^2 \bar{v}}{\partial \bar{r}^2} + \frac{1}{\bar{r}}\frac{\partial \bar{v}}{\partial \bar{r}} - \frac{\bar{v}}{\bar{r}^2} + \left(\frac{R_o}{Z_o}\right)^2 \frac{\partial^2 \bar{v}}{\partial \bar{z}^2}\right] \tag{7}$$

$$\frac{\partial \bar{u}}{\partial \bar{z}} + \left(\frac{\delta}{R_o}\right)\left(\frac{1}{\bar{r}}\right)\frac{\partial}{\partial \bar{r}}(\bar{r}\,\bar{v}) = 0 \tag{8}$$

The assumption is now made that $\frac{\delta}{Z_o} = \varepsilon << 1$ so that the slope of the protrusion is everywhere very small; the flow is

nearly one-dimensional. From Eq. 8 it is noted that $\frac{\partial \bar{u}}{\partial \bar{z}}$ is of the order of $\frac{\delta}{R_o}$, denoted symbolically as $\frac{\partial \bar{u}}{\partial \bar{z}} \sim 0(\frac{\delta}{R_o})$. Thus in Eq. 6 the last of the viscous terms is negligible with respect to the first two if $R_o \sim 0(Z_o)$. Therefore the component $\mu \frac{\partial^2 u}{\partial z^2}$ of the axial normal stress gradient is negligible compared to the gradient of the shear component. It is also assumed that $\frac{\partial \bar{p}}{\partial \bar{r}} << \frac{\partial \bar{p}}{\partial \bar{z}}$ so that the static pressure can be approximated by a function of z only; i.e., the pressure is uniform across the cross section of the tube. If the viscous terms are large with respect to the inertia terms in Eqs. 6 and 7 (small Re_o), then

$$\frac{\frac{\partial \bar{p}}{\partial \bar{r}}}{\frac{\partial \bar{p}}{\partial \bar{z}}} \sim 0 \left(\frac{\delta}{Z_o} \frac{R_o}{Z_o}\right) << 1$$

provided that $R_o \sim 0(Z_o)$. However if the inertia terms are large compared to the viscous terms (large Re_o) so that the right hand sides of Eqs. 6 and 7 may be neglected, then

$$\frac{\frac{\partial \bar{p}}{\partial \bar{r}}}{\frac{\partial \bar{p}}{\partial \bar{z}}} \sim 0 \left(\frac{\delta}{R_o}\right)$$

Therefore, for large Reynolds numbers, $\frac{\delta}{R_o}$ should be a small quantity in order to neglect the radial variation in pressure.

With the assumptions noted, Eqs. 6 and 7 in terms of the original variables become

$$u\frac{\partial u}{\partial z} + v\frac{\partial u}{\partial r} = -\frac{1}{\rho}\frac{\partial p}{\partial z} + \nu\left[\frac{\partial^2 u}{\partial r^2} + \frac{1}{r}\frac{\partial u}{\partial r}\right] \tag{9}$$

$$\frac{\partial p}{\partial r} = 0 \tag{10}$$

It can also be shown (see Appendix A) by the order-of-magnitude analysis that the wall shearing stress, τ_w, can be approximated by

$$\tau_w = \mu\frac{\partial u}{\partial r}\bigg|_{r=R} \tag{11}$$

so that separation or reattachment occurs when

$$\frac{\partial u}{\partial r}\bigg|_{r=R} = 0 \tag{12}$$

By making use of Eqs. 4 and 10, Eq. 9 can be rewritten as

$$\frac{\partial}{\partial z}(ru^2) + \frac{\partial}{\partial r}(ruv) = -\frac{r}{\rho}\frac{dp}{dz} + \nu\left[\frac{\partial}{\partial r}\left(r\frac{\partial u}{\partial r}\right)\right] \tag{13}$$

Equation 13 can now be integrated across the tube to eliminate the velocity component v. Leibnitz's Rule for differentration under a definite integral sign can be used since the functions ru^2, ruv, $\frac{\partial}{\partial z}(ru^2)$, and $\frac{\partial}{\partial z}(ruv)$ are assumed to be continuous in both r and z in $0 \leq r \leq R$, $-Z_o \leq z \leq Z_o$, and o and R (the limits of integration) are continuous and have continuous derivatives in $-Z_o \leq z \leq Z_o$. Making use of the boundary conditions u = v = o at r = R, and $\frac{\partial u}{\partial r} = 0$ at r = o, Eq. 13 becomes

$$\frac{d}{dz}\left[\int_o^R ru^2 dr\right] = -\frac{1}{\rho}\frac{dp}{dz}\frac{R^2}{2} + \nu R\left[\frac{\partial u}{\partial r}\right]_R$$

$$= -\frac{1}{\rho}\frac{dp}{dz}\frac{R^2}{2} + \frac{R}{\rho}\tau_w \qquad (14)$$

where Eq. 11 has been substituted into the right hand side of 14.

Equation 14 is an expression for the conservation of momentum. The left hand side arises from the non-linear convective acceleration terms in the equation of motion in the z - direction. In effect, Eq. 14 shows that the mean sectional kinetic energy gradient (due to the inertia of the fluid) is equal to the driving force on the fluid minus the drag force exerted by the wall on the fluid.

Equation 14, together with the continuity equation written in the form

$$Q = \pi R^2 \bar{U} = \int_o^R 2\pi r u dr \qquad (15)$$

where $\bar{U}$ is the mean velocity at any given cross section with radius R and Q is some constant volume rate of flow, are sufficient to describe the flow. The radius R is assumed to be a known function of z, and the particular geometry studied is the stenosis described by Eq. 1.

An exact solution for Eqs. 1, 14, and 15 has not been obtained. Instead, it is assumed that the radial dependence of the axial velocity can be expressed by a fourth order polynomial of the form

$$\frac{u}{U} = A\left(\frac{R-r}{R}\right) + B\left(\frac{R-r}{R}\right)^2 + C\left(\frac{R-r}{R}\right)^3 + D\left(\frac{R-r}{R}\right)^4 + E \qquad (16)$$

where U is the centerline velocity and A through E are undetermined coefficients. This is similar in form to that assumed in the Karman-Polhausen analysis of two-dimensional boundary layer equations. However, it should be emphasized that the present problem is not a boundary layer problem in the sense of having a potential core of fluid outside of the boundary layer.

The coefficients in Eq. 16 are evaluated from the following five conditions:

a) at $r = R$, $u = o$

b) at $r = o$, $\frac{\partial u}{\partial r} = o$

c) at $r = o$, $u = U$ (17)

d) at $r = R$, $\frac{dp}{dz} = \mu\left(\frac{\partial^2 u}{\partial r^2} + \frac{1}{r}\frac{\partial u}{\partial r}\right)$

e) at $r = o$, $\frac{\partial^2 u}{\partial r^2} = -\frac{2U}{R^2}$

The boundary conditions of zero velocity (no slip) at the walls and axisymmetric flow are given by (a) and (b). Condition (c) is simply a definition, and (d) is obtained from Eq. 9. In order to obtain the fifth condition (e) it is assumed that at $r = o$, the velocity profile is very nearly parabolic at the center of the tube ($u = U[1 - (\frac{r}{R})^2]$) so that the second derivative of u with respect to r, at $r = o$, can be approximated by (e). Intuitively, it is felt that only near

the wall of the tube will the velocity profile deviate significantly from the parabolic form.

In order to satisfy these five conditions the coefficients in Eq. 16 must be given by the relations

$$A = \frac{-\lambda + 10}{7} \qquad B = \frac{3\lambda + 5}{7} \qquad C = \frac{-3\lambda - 12}{7}$$

$$D = \frac{\lambda + 4}{7} \qquad E = 0 \tag{18}$$

where

$$\lambda = \frac{R^2}{\mu U} \frac{dp}{dz}$$

Thus Eq. 16 becomes

$$\frac{u}{U} = \left(\frac{-\lambda + 10}{7}\right)\left(\frac{R-r}{R}\right) + \left(\frac{3\lambda + 5}{7}\right)\left(\frac{R-r}{R}\right)^2 + \left(\frac{-3\lambda - 12}{7}\right)\left(\frac{R-r}{R}\right)^3 + \left(\frac{\lambda + 4}{7}\right)\left(\frac{R-r}{R}\right)^4 \tag{19}$$

It is noted that λ is a function of z only since R, U, and p depend only on z. Equation 19 can be substituted into Eq. 15 (the continuity equation) which is then integrated to give

$$Q = \frac{\pi R^2}{210}\left[97U - \frac{2R^2}{\mu}\frac{dp}{dz}\right] \tag{20}$$

Also the expression for U in terms of the pressure gradient is

$$U = \frac{210}{97\pi}\frac{1}{R^2}\left[Q + \frac{\pi}{105\mu} R^4 \frac{dp}{dz}\right] \tag{21}$$

Finally, Eqs. 19 and 21 can be substituted into the momentum equation (Eq. 14) and after a considerable amount of straight-forward integrations and simplification of terms one

obtains the relation

$$\rho\left\{\frac{c_1+c_2c_5+c_3c_5^2}{\mu^2}\right\}\left\{6R^5\,\frac{dR}{dz}\left(\frac{dp}{dz}\right)^2 + 2R^6\,\frac{dp}{dz}\,\frac{d^2p}{dz^2}\right\}$$
$$+\ \rho\left\{\frac{c_2c_4Q+2c_3c_4c_5Q}{\mu}\right\}\left\{2R\frac{dR}{dz}\,\frac{dp}{dz} + R^2\,\frac{d^2p}{dz^2}\right\}$$
$$-\ \rho\{c_3c_4^2Q^2\}\left\{2R^{-3}\,\frac{dR}{dz}\right\} + \frac{10}{7}\,\frac{\mu c_4Q}{R^2}$$
$$+\ \frac{20c_5+5}{14}\,R^2\,\frac{dp}{dz} = 0 \qquad (22)$$

where

$$c_1 = \frac{1}{17640} \qquad c_2 = -\frac{1}{252} \qquad c_3 = \frac{661}{4410} \qquad (23)$$
$$c_4 = \frac{210}{97\pi} \qquad c_5 = \frac{2}{97}$$

and R is given by Eq. 1.

Equation 22 is a first order non-linear ordinary differential equation in terms of the pressure gradient. Ideally, one would like to solve Eq. 22 for $\frac{dp}{dz}$ in terms of z. This result could then be substituted back into Eqs. 21 and 19, and the velocity profile as a function of r and z would be obtained. One could then calculate the wall shearing stresses and the separation and reattachment points could be determined. A final integration of $\frac{dp}{dz}$ would give the pressure along the stenosis as a function of z.

However, it is not apparent how an exact solution can be obtained for Eq. 22. Rather than solving it numerically and

then proceeding as discussed above, it was decided to make one more approximation in the momentum equation in order to obtain a closed form solution to the problem.

The non-linearities in Eq. 22 are contained in the bracketed terms, which arise from the integral in the momentum equation (Eq. 14). If the bracketed terms are neglected, the flow thus described will be a "Poiseuille" flow through the stenosis, a situation already discussed by Young (3). In the present study, instead of neglecting the integral, it is evaluated by assuming that the velocity profile is parabolic

$$u = 2\bar{U}\left[1 - \left(\frac{r}{R}\right)^2\right] \qquad (24)$$

where $\bar{U}$ is the mean velocity at the given cross section. It is noted that the assumed profile satisfies the boundary conditions $\left.\frac{\partial u}{\partial r}\right|_{r=0} = o$ and $u = o$ at $r = R$. Barnard, et al. (34) in their study of unsteady flow through felxible tubes evaluated this same integral by such an approximation. This procedure in effect combines the concept of "successive approximations" with the momentum-integral technique, in the sense that the parabolic velocity distribution is the first approximation to the problem. For mild stenoses, the velocity profile is known to approach the parabolic distribution for low Reynolds numbers. Thus the validity of the assumption is expected to increase as the Reynolds number is decreased.

Substitution of Eq. 24 into the left hand side of Eq. 14 and evaluation of the integral reduces the momentum equation to

$$\frac{d}{dz}\left(\frac{2}{3} R^2\bar{U}^2\right) = -\frac{1}{\rho}\frac{dp}{dz}\frac{R^2}{2} + \nu R\frac{\partial u}{\partial r}\bigg|_R \qquad (25)$$

Since $\bar{U} = \frac{Q}{\pi R^2}$ (Eq. 15), Eq. 25 can be written as

$$-\frac{4}{3}\frac{Q^2}{\pi^2}\frac{1}{R^3}\frac{dR}{dz} = -\frac{1}{\rho}\frac{R^2}{2}\frac{dp}{dz} + \nu R\frac{\partial u}{\partial r}\bigg|_R \qquad (26)$$

The derivative of the velocity $(\partial u/\partial r)_R$ as obtained by Eq. 19 can be substituted into Eq. 26 to give

$$-\frac{4}{3}\frac{Q^2}{\pi^2}\frac{1}{R^3}\frac{dR}{dz} = -\frac{1}{\rho}\frac{R^2}{2}\frac{dp}{dz} + \frac{\nu}{7}\left[\frac{R^2}{\mu\bar{U}}\frac{dp}{dz} - 10\right][U] \qquad (27)$$

Finally, substitution of Eq. 27 into Eq. 21, yields for the pressure gradient,

$$\frac{dp}{dz} = \frac{5432}{1575\pi^2}\frac{\rho Q^2}{R^5}\frac{dR}{dz} - \frac{8\mu Q}{\pi R^4} \qquad (28)$$

The first term on the right hand side represents the contribution due to the inertia of the fluid. In the converging portion of the tube, $\frac{dR}{dz}$ is negative so that a favorable pressure gradient exists. However, in the diverging portion $\frac{dR}{dz}$ is positive so that an adverse pressure gradient $(\frac{dp}{dz} > 0)$ may develop. In dimensionless form Eq. 28 becomes (after substitution for Q in terms of $\bar{U}_o$ and R_o)

$$\frac{R_o}{\rho\bar{U}_o^2}\frac{dp}{dz} = \frac{5432}{1575}\frac{R_o^5}{R^5}\frac{dR}{dz} - \frac{16}{Re_o}\frac{R_o^4}{R^4} \qquad (29)$$

where

$$Re_o = \frac{2R_o\bar{U}_o}{\nu} \tag{30}$$

is the Reynolds number upstream from the stenosis. Thus, in order for $\frac{dp}{dz} \geq 0$, i.e., an adverse pressure gradient to develop, the following condition must hold:

$$\frac{5432}{1575}\frac{R_o}{R}\frac{dR}{dz} \geq \frac{16}{Re_o}$$

or

$$Re_o\frac{R_o}{R}\frac{dR}{dz} \geq \frac{3150}{679} \tag{31}$$

When R is defined by Eq. 1, $\frac{1}{R}\frac{dR}{dz}$ will have its maximum value somewhere near the middle of the diverging section, and there will be some minimal value of Re_o in order for Eq. 31 to hold. As Re_o is increased above this minimum value, $\frac{1}{R}\frac{dR}{dz}$ can be decreased and Eq. 31 will still hold. Thus the region of adverse pressure gradient will extend both upstream and downstream in the diverging portion of the tube as the Reynolds number is increased.

Equations 21 and 28 can be substituted into Eq. 19 to give the velocity u as a function of r and z.

$$\frac{u}{\bar{U}_o} = Re_o\left(\frac{R_o}{R}\right)^3\frac{dR}{dz}\left[-\frac{308}{1575}\left(\frac{R-r}{R}\right) + \frac{1204}{1575}\left(\frac{R-r}{R}\right)^2 - \frac{4}{5}\left(\frac{R-r}{R}\right)^3 + \frac{4}{15}\left(\frac{R-r}{R}\right)^4\right]$$

$$+ 2\left(\frac{R_o}{R}\right)^2\left[1 - \frac{r^2}{R^2}\right] \tag{32}$$

The velocity profiles along the stenosis may now be plotted, as shown in the next chapter.

Substitution of Eq. 32 into Eq. 11 for the wall shearing stress gives

$$\tau_w = \mu\bar{U}_o\left[\frac{308}{1575}\frac{Re_o}{R}\left(\frac{R_o}{R}\right)^3\frac{dR}{dz} - \frac{4}{R}\left(\frac{R_o}{R}\right)^2\right] \tag{33}$$

In dimensionless form Eq. 33 becomes

$$\frac{\tau_w}{\rho\bar{U}_o^2} = \frac{616}{1575}\frac{R_o^4}{R^4}\frac{dR}{dz} - \frac{8}{Re_o}\frac{R_o^3}{R^3} \tag{34}$$

The separation and reattachment points occur where $\left.\frac{\partial u}{\partial r}\right|_R = 0$; i.e. where the wall shearing stress is zero. Therefore the separation-reattachment condition is

$$\frac{616}{1575}\frac{R_o}{R}\frac{dR}{dz} = \frac{8}{Re_o}$$

or

$$Re_o\frac{R_o}{R}\frac{dR}{dz} = \frac{225}{11} \tag{35}$$

For the case of incipient separation, i.e., the Reynolds number is just large enough to cause separation, it is desirable to know where in the diverging portion separation will begin. To determine this point $\frac{1}{R}\frac{dR}{dz}$ is maximized with respect to z. Thus

$$\frac{d}{dz}\left(\frac{1}{R}\frac{dR}{dz}\right) = \frac{RR''-(R')^2}{R^2} = 0 \tag{36}$$

Use is now made of the expression for R (Eq. 1) and the location of the initial separation point is given by the relation

$$\frac{z}{z_o} = \frac{1}{\Pi}\ \text{arcsec}\ \left(\frac{2R_o}{\delta} - 1\right) \tag{37}$$

For $R_o = 3\delta$ (the geometry studied experimentally)

$$\frac{z}{Z_o} = 0.435 \tag{38}$$

It is noted from Eq. 37 that for the geometry described by Eq. 1 the initial separation point $\frac{z}{Z_o}$ is only a function of $\frac{R_o}{\delta}$ and does not depend on Z_o. However, in general the separation and reattachment points will depend upon both the ratios of $\frac{R_o}{\delta}$ and $\frac{Z_o}{\delta}$ as can be easily seen by substituting Eq. 1 into Eq. 35.

Once the incipient separation point is evaluated by Eq. 38, the critical Reynolds number required to produce separation can be evaluated from Eq. 35. For the geometry $Z_o = 4R_o = 12\delta$, the critical Reynolds number is 127.5.

As the Reynolds number increases above the critical value to cause separation, Eq. 35 is satisfied by two values of z; the smaller value of z gives the separation point and the larger value gives the reattachment point. As the Reynolds number increases, the separation point moves upstream and the reattachment point moves downstream. However, based on the present theory, the entire separation region will always be contained in the diverging portion, for $\frac{dR}{dz} \to 0$ as $z \to 0$ or as $z \to Z_o$. As the Reynolds number becomes large, one expects the reattachment point to move downstream from the stenosis. Therefore the theory definitely cannot hold for any values of Reynolds numbers which experimentally are great enough to cause the reattachment point to be beyond

Z_o. Actually it is expected that the theoretical solution will become inaccurate before this condition is reached.

In comparing Eqs. 31 and 35, it is noted that the pressure gradient becomes positive before separation occurs. For a given Re_o and R_o, the required value of $\frac{1}{R}\frac{dR}{dz}$ for separation is approximately four times greater than its value for an adverse pressure gradient to be developed. Thus the existence of a positive pressure gradient does not necessarily imply that separation will occur. Before separation can occur, the adverse pressure gradient must grow to such a size that it can overcome both the inertia and viscous effects of the fluid near the wall.

Ideally, under steady flow conditions, there is no flow of fluid into or out of the separation region. Thus an equation for the stream surface enclosing the separation region may be obtained from the equation

$$Q = \int_o^{R_1} 2\pi r u dr \tag{39}$$

where R_1 is the radial distance from the centerline of the tube to the stream surface. When the expression for u (Eq. 32) is substituted into Eq. 39, the equation to be solved for R_1 becomes

$$1 = Re_o \frac{R_o}{R^3}\frac{dR}{dz}\left[\frac{56}{1575} R_1^2 - \frac{4}{225}\frac{R_1^4}{R^2} - \frac{8}{75}\frac{R_1^5}{R^3} + \frac{4}{45}\frac{R_1^6}{R^4}\right] + \frac{2}{R^2}\left[R_1^2 - \frac{R_1^4}{2R^2}\right]$$

or, after factoring

$$0 = \left(\frac{R_1}{R} - 1\right)^2 \left\{\frac{28}{1575} Re_o \frac{R_o}{R} \frac{dR}{dz}\left[5\left(\frac{R_1}{R}\right)^4 + 4\left(\frac{R_1}{R}\right)^3 + 2\left(\frac{R_1}{R}\right)^2\right]\right.$$

$$\left. - \left(\frac{R_1}{R} + 1\right)^2\right\} \qquad (40)$$

The two roots at $\frac{R_1}{R} = 1$ are of no interest, so that the final form of the equation to be solved for R_1 becomes

$$0 = \frac{28}{1575} Re_o \frac{R_o}{R} \frac{dR}{dz}\left[5\left(\frac{R_1}{R}\right)^4 + 4\left(\frac{R_1}{R}\right)^3 + 2\left(\frac{R_1}{R}\right)^2\right] - \left(\frac{R_1}{R} + 1\right)^2 \qquad (41)$$

The above expression will be used in Chapter V to draw the streamlines enclosing the separation regions in Fig. 10.

To obtain the pressure p at any cross section z along the stenosis, Eq. 28 must be integrated, using the boundary condition that $p = p_o$ at $z = -Z_o$. Upon performing the integration (see Appendix B) one obtains in dimensionless form

$$\frac{p-p_o}{\rho \bar{U}_o^2} = -\frac{1358}{1575} R_o^4 \left\{\frac{1}{\left[R_o - \frac{\delta}{2}\left(1 + \cos\frac{\pi z}{Z_o}\right)\right]^4} - \frac{1}{R_o^4}\right\}$$

$$- \frac{32}{\pi} \frac{Z_o}{R_o} \frac{1}{Re_o} \left\{\frac{1}{\sqrt{c}} \arctan\frac{x}{\sqrt{c}} + 3(1-c)\left[\frac{x}{2c(c+x^2)} + \frac{1}{2c\sqrt{c}} \arctan\frac{x}{\sqrt{c}}\right]\right.$$

$$+ \frac{3(1-c)^2}{4c}\left[\frac{x}{(c+x^2)^2} + \frac{3x}{2c(c+x^2)} + \frac{3}{2c\sqrt{c}} \arctan\frac{x}{\sqrt{c}}\right]$$

$$+ \frac{(1-c)^3}{6c}\left[\frac{x}{(c+x^2)^3} + \frac{5x}{4c(c+x^2)^2} + \frac{15x}{8c^2(c+x^2)} + \frac{15}{8c^2\sqrt{c}} \arctan\frac{x}{\sqrt{c}}\right]$$

$$\left. + \frac{\pi}{2}\left[\frac{1}{\sqrt{c}} + \frac{3(1-c)}{2c\sqrt{c}} + \frac{9(1-c)^2}{8c^2\sqrt{c}} + \frac{5(1-c)^3}{16c^3\sqrt{c}}\right]\right\} \qquad (42)$$

where

$$Re_o = \frac{2\bar{U}_o R_o}{\nu} \qquad x = \tan \frac{\Pi z}{2Z_o} \qquad c = 1 - \frac{\delta}{R_o} \tag{43}$$

The first bracketed term on the right hand side of Eq. 42 denotes the pressure drop due to the changing kinetic energy of the fluid as it flows through the converging-diverging section. At the downstream end of the stenosis ($z=Z_o$) this first term becomes zero.

The remaining terms in Eq. 42 arise from the viscous effects of the fluid and do contribute to the over-all pressure drop across the stenosis. Letting z approach Z_o in Eq. 42 gives this pressure drop as

$$\left(\frac{p-p_o}{\rho \bar{U}_o^2}\right)_T = -\frac{32}{Re_o}\frac{Z_o}{R_o}\left\{\frac{1}{\sqrt{c}} + \frac{3(1-c)}{2c\sqrt{c}} + \frac{9(1-c)^2}{8c^2\sqrt{c}} + \frac{5(1-c)^3}{16c^3\sqrt{c}}\right\} \tag{44}$$

where the subscript T denotes the total pressure drop across the stenosis and Re_o and c are defined by Eq. 43. If there is no constriction in the tube, then c = 1 and Eq. 44 reduces to the expression obtained for Poiseuille flow, where Z_o is one half of the length over which the pressure drop is computed.

To conclude this chapter, a comparison will be made between the results obtained herein and those obtained by Blasius (Sec. A2 of Chapter II) for flow in a slightly diverging tube. Caution should be used in applying Blasius' results to the present investigation since $\frac{d^2R}{dz^2}$ is not

necessarily an order-of-magnitude smaller than $\frac{dR}{dz}$ (it would be near the point $z = \frac{z_o}{2}$). However, comparisons can be made between the expressions for the pressure gradient in the axial direction, the velocity profile, and for the separation-reattachment condition. Blasius' equation for the pressure gradient is identical in form with Equation 28 of the present analysis. In fact, the only difference between the two equations is that the constant 4 in the inertia term of Blasius' expression is replaced by $\frac{5432}{1575}$ in Eq. 28. Blasius' expression for the axial velocity is of the same form as Eq. 32, in that both expressions consist of a parabolic term plus a "corrective" term which is a polynomial in r/R. The difference between the two expressions is in the polynomial. Blasius uses the same condition for separation as used in this investigation. However, if one thinks of applying his relation to the converging-diverging tube problem, then Blasius' condition for separation and reattachment is

$$Re_o \frac{R_o}{R} \frac{dR}{dz} = 12$$

where Re_o is the Reynolds number based on upstream conditions (at $R = R_o$). This is the exact form of relationship that is obtained in the present investigation (Eq. 34), but the constant 12 is considerably smaller than $\frac{225}{11}$ obtained in Chapter III. Thus for a given $\frac{R_o}{R} \frac{dR}{dz}$ the Blasius' solution would predict separation at a Reynolds number approximately

0.6 of the Reynolds number required to cause separation in the present analysis.

IV. EXPERIMENTAL PROCEDURE

A. Description of Apparatus

The separation phenomenon and the pressure drop across a stenosis were studied for water, various glycerol-water solutions, and blood in a 17.7-inch long, rigid, plastic tube having a uniform diameter of 0.750-inch in the straight portion (see Figs. 3 and 4). Figure 3 is a photograph of the entire plastic tube, including its end connections. Figure 4 shows the tube with bovine blood flowing through it.

The converging-diverging section of the tube was 3.00 inches long (Z_o = 1.50 in.) and the minimum diameter (the throat diameter) was 0.500 inch. The stenosis was constructed to satisfy the geometry studied theoretically (Eq. 1) so that in terms of the geometry shown in Fig. 2, $Z_o = 4R_o = 12\delta$ for the experimental test section. The method used to make the tube will be described at the end of this section.

A series of 0.026-inch diameter holes were drilled along the tube so that dye or suspensions of small particles could be injected at various stations in order to study the separation phenomena and to measure the pressure drops along the wall. The holes were counterdrilled for number 19-gauge hypodermic needles. The needles were glued into the tube and connected to stopcocks by short pieces of latex rubber tubing. The flexible tubing prevented the glued joints from being broken when connections were made to the stopcocks.

Figure 3. Plastic converging-diverging tube

Figure 4. Bovine blood flowing through tube

Figure 5. Test apparatus

A photograph of the entire test apparatus is shown in Fig. 5. The upstream and downstream portions of the plastic test section were connected to 0.750-inch brass tubing having lengths of 24 and 14.75 inches respectively. The ends of the plastic test section were bored to receive the brass tubing so that a smooth transition from the brass to the plastic tubing was obtained (Fig. 3). Thus, an "entrance length" of straight 0.75-inch diameter tubing 30.4 inches long preceded the converging-diverging section. According to Goldstein (20, p. 301) this length is sufficient so that a fully developed laminar flow is obtained before reaching the stenosis for Reynolds numbers up to approximately 1400.

As shown in Fig. 5, the upstream portion of the brass tubing was connected to a constant-head tank by 0.875 inch diameter tygon tubing. The liquid flowed from the downstream portion of the brass tubing back to a reservoir by means of 0.375-inch tubing. The liquid was pumped from the reservoir up to the constant-head tank at a rate sufficient to always provide some overflow back to the reservoir, so that a constant head supply was maintained. The amount of fluid flowing through the converging-diverging tube was controlled by means of an adjustable clamp on the tygon tubing leading to the reservoir. The flow rate was determined by measuring the time required to collect a given volume of fluid.

Two types of variable speed pumps were used in the

experiments. A Sigmamotor "finger" pump which was manufactured to pump blood through a Travenol artificial kidney was used in the experiments using water and glycerol-water solutions. This pump is shown in the photograph of Fig. 5, and had a maximum output of approximately 0.85 liters per minute. Therefore, maximum Reynolds numbers of approximately 1100 could be obtained when using water in the system. However, when blood, having a kinematic "viscosity" approximately six times that of the water, was put into the system the maximum Reynolds number was reduced by a factor of six. Therefore, a Sarns Model 3500 portable roller pump was used in the experiments involving blood as it provided flows up to 4.8 liters per minute. Therefore, pressure drops and separation phenomena could be studied over the same range of Reynolds numbers as used with the water. Both pumps were selected in preference to other types of pumps available because they produce a minimal amount of hemolysis of blood during the pumping process. However, the "finger" pump was not used in the tests involving blood.

The transparent plastic tube, which contained a converging-diverging section as discussed in the first part of this chapter, was cast around a smooth brass rod using Natcol[1]

---

[1]Natcol Plastics, Redlands, California.

NL-410 clear polyester casting resin. The 0.750-inch diameter solid brass rod was first cut into two pieces with a threaded connection between the two sections. The converging-diverging geometry was then machined, with the minimum diameter at the junction between the two pieces of rod. Although the rod was very carefully machined, the geometry obtained did not coincide precisely with that described by Eq. 1 of Chapter III:

$$R = R_o - \frac{\delta}{2}\left(1 + \cos\frac{\Pi z}{z_o}\right)$$

In what was later used as the converging portion of the tube, the actual radius at any given cross section was within 5% of that specified by Eq. 1. In the diverging section the radius was within 3% of the desired value.

Before making the casting, the polished brass rod was first coated with a very thin layer of silicone grease. Removal of the rod from the hardened plastic was facilitated by heating in an oven at approximately 75° C. The casting, which was made with a square cross section as seen in Figs. 3 and 4, was milled and then polished on the outside to improve its optical properties. The 0.026-inch diameter holes were carefully drilled so that no burr would be left on the inside of the tube. The holes were spaced at 0.25-inch intervals along the stenosis (0.50-inch intervals on each side). As a final precaution to prevent any small burrs from remaining, the inside of the tube was polished.

B. Acquisition of Data

The flow characteristics studied experimentally were the separation and reattachment points and the pressure drop across the stenosis. The major portion of the experimental work was carried out with distilled water or various concentrations of glycerol-water solutions, although human blood and bovine blood were also used after the procedures for obtaining the data were established.

The temperature, specific gravity, and kinematic viscosity of the fluid were measured and recorded at various times throughout each experimental run. All experiments were performed at room temperatures, which ranged from 22° to 27° C over the entire period for the test program. The temperature of the fluid did not vary more than 1.0° C during any given test, and when a temperature variation did occur, the change in the viscosity of the fluid was taken into account.

1. Viscosity measurements

The kinematic viscosity of the glycerol-water solutions and the apparent kinematic viscosity of the blood were determined by means of two Cannon-Fenske Viscometers (No. 50 and No. 100). In this method of viscosity measurement the time is recorded for a given volume of fluid to flow through a capillary tube. Relative values of kinematic viscosity are obtained by comparing liquids having an unknown viscosity

with a standard having a known viscosity. Distilled water was the standard liquid used in these experiments.

Blood is not a Newtonian fluid. However, as mentioned in Chapter I, many researchers feel that blood behaves as a Newtonian fluid except at very low rates of shear. Merrill (13) states that the stress range of most capillary viscometers falls in the region of Newtonian behavior of blood (above shearing strain rates of 100 per sec.).

Using the Cannon-Fenske viscometer, the kinematic viscosity of citrated whole human blood (type O positive) at 24° C was 0.0550 stokes. The blood was a combination of 4 pints of type O positive and one pint of type O negative and had a specific gravity of 1.046. It was approximately three months old and had a hematocrit of 32. Since normal human blood has approximately 35-45% by volume red blood cells, deterioration of the red blood cells had occurred. This was further evidenced by the brightly colored red plasma which was observed when the blood was centrifuged, indicating that plasma hemoglobin was abnormally high. The absolute viscosity of the human blood was 0.0575 poise at 24° C. Merrill (13) states that the normal value is between 0.03 and 0.04 poise for human blood at 37° C.

Fresh bovine blood was also used in the experiments. Six liters of the blood were obtained, to which 150 mg. of sodium heparin was added to prevent clotting. The blood had a

specific gravity of 1.054, a hematocrit of 43%, and an ultimate kinematic viscosity of 0.0573 stokes at 24° C. Thus its absolute viscosity was 0.0604 poise. In order to prevent clotting in the wall taps, another 150 mg. of heparin was added when the pressure drops were measured. The viscosity was then checked again and did not differ from its previous value.

2. Separation and reattachment measurements

The primary purpose of the experimental investigation of flow through a converging-diverging tube was to determine at what minimum Reynolds number separation occurred in the diverging portion of the tube, and to observe where the region started and ended at larger Reynolds numbers. A Nikon Stereoscopic Microscope (Model SMZ-2) was used to observe the flow near the wall when it was advantageous to do so.

Several different methods of observing the backflow of fluid near the wall of the tube were employed when using either distilled water or glycerol-water solutions in the system. These methods will be discussed and illustrated in the remainder of this section, starting with the procedure which was used to obtain all the data shown on the experimental curves in Fig. 12 of the next chapter. In Fig. 12 the separation and reattachment points are plotted verses the Reynolds

number of the flow for the converging-diverging tube studied experimentally ($Z_o = 4R_o = 12\delta$). It is believed that the following procedure which was used to obtain these separation and reattachment points involved the least amount of personal judgement of the different methods tried. This procedure was also applicable in defining the separation region when using blood in the system. Since the results for blood and the Newtonian fluids were to be compared, it was desirable to use the same method for all fluids studied.

Dye was injected very slowly in the separation region through the wall taps at various positions downstream from the throat of the stenosis. The separation point was defined as the point nearest the throat where a reversed flow along the inside wall of the tube occurred. The point furthest downstream from the throat where backflow occurred was defined as the reattachment point. The dye was injected at a rate just sufficient to produce a thin filament along the wall of the tube, so that the direction of flow could be observed. Usually the data was taken with the wall taps lying in a horizontal plane as shown in Figs. 3,4, and 5, but the plastic tube could be rotated to any angle desired with no apparent change in the flow characteristics.

The dyes used were made by mixing aniline blue (dark blue) or potassium permangamate (dark red) with water, or saline depending on whether water, or blood was flowing

through the converging-diverging tube. Both anilene blue and potassium permangamate are readily dissolvable in water or saline, and thus very concentrated dye solutions could be obtained.

The method just presented of obtaining data for the separation and reattachment points will be discussed further in Chapter V, when the experimental results are discussed. The method is illustrated in Fig. 6. In Fig. 6 the wall taps lie in a horizontal plane, and the view is from an approximately 30 degree angle with this plane. Bovine blood is flowing through the tube from right to left at a Reynolds number of 850, based on upstream conditions. Dark blue dye is being injected from a tap 2.5 inches downstream (arrow A) from the throat (arrow B) of the constriction. The dye has moved along the boundary back to a position approximately 0.55 inches from the throat (arrow C). Thus the separation point is at $z/Z_o = 0.367$. The movement upward of the slowing moving dye stream as it approaches the separation point is due to the fact that the specific gravity of the dye solution is 1.006 while that of the blood is 1.046.

Figure 7 is a photograph of the test section with water flowing through the system at a Reynolds number of 600. The flow is from left to right, and the dark region near the lower wall in the diverging portion is the separation region. The dark lines near the upper walls were produced by shadows.

Figure 6. Separation at a Reynolds number of 850

Figure 7. Separation at a Reynolds number of 600

Figure 8. Separation at a Reynolds number of 900

Figure 9. Separation at a Reynolds number of 1200

In this particular case red dye is being injected through a downstream tap 1.5 inches (arrow A) from the throat. The dye has moved upstream to a point approximately 0.65 inches from the throat (the separation point, arrow B) and then has been carried by the forward moving fluid in the separation region to a point approximately 2.2 inches from the throat (the reattachment point, arrow C). This method of injecting dye near the center of the separation region has the advantage that the flow near the end points of the separation region is not disturbed by the injected dye. However, it is difficult to define a reattachment point as some of the dye moves out of the separation zone and flows on downstream. In some cases blue dye was injected from a tap one inch upstream from the throat (arrow D in Fig. 7). The blue filament of dye proceeded downstream along the streamline which enclosed the separation region, and thus helped to establish the reattachment point. The thickness of the separation region can be estimated from Fig. 7, but it must be remembered that there is a blue stream of dye running along the top of the region.

The photograph in Fig. 8 shows dye being injected on both sides of the tube in the converging portion (arrows A). Both streams of dye separate from the wall (arrows B) approximately 0.55 inches from the throat and reattach to the wall between 3.0 and 3.5 inches from the throat (arrows C).

The stereomicroscope was used when taking data in this manner to help determine where the streamline of dye left the wall and where it again made contact with the wall. The Reynolds number of the flow shown in Fig. 8 is approximately 900, which is near the upper limit which will still give a well defined laminar separation region. A few data points for separation and reattachment obtained in this manner are plotted in Fig. 13 of Chapter V in order to compare the results with those obtained by injecting inside the separation region. These results will be discussed in the next chapter.

Figure 9 shows the flow of water (left to right) through the converging-diverging tube at a Reynolds number sufficiently high (1200) to produce turbulence in the separation region. As in Fig. 8, dye was injected on both sides in the converging portion. At a Reynolds number of approximately 1200, the stream of dye begins to become somewhat wavy near the position $z/Z_o = 1.3$ as seen in Fig. 9 (arrows A). As the Reynolds number is further increased to approximately 1800, the turbulent separation region extends both upstream to the separation point and downstream. The dye very rapidly circulates around the entire tube, but is still concentrated near the walls of the tube, rather than being evenly distributed across the total cross section.

Figures 8 and 9 indicate that the separation region was

reasonably axisymmetric. This indeed was the case for the range of Reynolds numbers studied.

Another method used to define the separation region was to inject very rapidly a large quantity of dye into the diverging portion of the tube and to observe after a period of time the region which still contained dye. This method showed very clearly the axial symmetry of the separation region. A difficulty with the above procedure is that the fluid near the wall of the tube is moving very slowly, especially near the separation and reattachment points. Therefore, a sufficient amount of time must be allowed in order for the dyed fluid outside of the separation region to move on downstream. However, during this same time dye is diffusing out of the separation region. Thus the end points are difficult to define, especially the reattachment point.

Since the separation region is extremely thin near the separation and reattachment points, it was felt that the data obtained by injecting the dye into the separation region was somewhat conservative in the sense that separation may have occurred slightly upstream from the point where the dye could be seen to have "backflow". Reattachment was determined by noting how far downstream dye could be injected and still obtain backflow, but the injection of the dye at a non-zero velocity caused at least a small disturbance of the flow near the wall. Also, the film of dye had to have

some finite thickness before it could be seen. Therefore, a brief investigation was made in which suspensions of small particles were injected into the separation region, the converging portion of the tube, or added to the entire fluid (water or glycerol-water solutions). The paths of these particles in the plastic tube were followed, using the stereomicroscope for observing the smaller particles.

Various types and sizes of particles were added to different concentrations of glycerol-water solutions, in an attempt to keep the small particles in suspension. Suspensions of the particles were then injected into the converging-diverging tube, which contained a glycerol-water solution of the same concentration as that used for suspending the particles. A basic difficulty was to obtain a particle of sufficiently small size to stay in suspension and not disrupt the flow near the walls of the tube, and at the same time, to be able to follow the paths of individual particles with the aid of the stereomicroscope.

Three different types of particles whose movement could be traced through the plastic tube were Herter's Lamiset[1] (a white powered catalyst), Amberlite IRA-93[2] synthetic ion

---

[1]Herter's, Inc., Waseca, Minn.

[2]Rohm and Haas Company, Philadelphia, Pennsylvania, 19105.

exchange resin, and Mearlin-A Pearl[1] (a nacreous pigment) consisting of mica flakes coated with titanium dioxide). Backflow of the powdered catalyst, when suspended in water, and the resin, when suspended in a glycerol-water solution, was observed at Reynolds numbers between 500 and 1000. However, the end points of the backflow regions generally fell inside the separation region defined by dye injection, and consistent data points were not obtained for given Reynolds numbers. Backflow of Mearlin-A particles suspended in a glycerol-water solution (25% glycerol by volume) was observed at Reynolds numbers as low as 330. The longest dimension of the Mearlin-A particles was from 2 to 20 microns, so it was difficult to distinguish between individual particles. Nevertheless, some backward movement was observed in the range of z/Z_o = 0.53 to 1.16 at a Reynolds number of 330. This pair of values for separation and reattachment and two other pairs obtained at higher Reynolds numbers are within 15% of those values obtained for water by injecting dye in the separation region. Thus for the particles studied, the Mearlin-A gave the most consistent results, which also happened to agree most closely with the results already obtained by injecting the dye.

Since no new information was obtained in the preliminary

---

[1]The Mearl Corporation, 41 East 42nd Street, New York 17, N.Y.

investigations using different particles, it was decided not to pursue this method further. To do so would require improved visualization techniques, smaller particles, and more refined methods of keeping the particles in suspension.

3. Pressure drop measurements

The pressure drop was measured by attaching two pieces of 0.375-inch diameter tygon tubing to two wall taps (each 6.0 inches from the throat) and recording the heights of the two columns of fluid with a traveling microscope having a least count of 0.0001 inch. Data were obtained for pressure drops when both water and heparinized bovine blood were used as the fluids. Pressure drops were extremely small when water was flowing through the system (0.003 and 0.013-inches of water for Reynolds numbers of 500 and 1000, respectively); thus it was necessary to eliminate as much as possible the effects of surface tension on the height of the water columns. This was accomplished by using the 0.375-inch tygon tubing for the two piezometer tubes, as evidenced by a very small meniscus in each tube. Values of pressure drops were recorded at various Reynolds numbers up to 1030 for the distilled water (see Fig. 17 in the next chapter). Approximately 25 minutes was spent at each data point in order to allow the water in each piezometer tube to reach its equilibrium position. Two runs were made, and the values obtained for pressure

drops were within 0.0025 inches of water at corresponding Reynolds numbers.

Pressure drops were also measured when bovine blood was flowing through the system. Because the kinematic viscosity of the blood was approximately six times that of the water, pressure drops at a given Reynolds number were approximately 36 times those obtained when using water (see Eq. 44, Chapter III). Approximately 3 to 5 minutes was allowed for the blood in the piezometer tubes to reach its equilibrium level for a given flow rate through the tube. Before changing to a new flow rate, the blood in the piezometer tubes was oscillated in order to "wash out" the small openings in the wall taps. It appeared that clotting in the wall taps was prevented by this procedure. The difference in heights between the two columns of fluid in the piezometer tubes was measured with a scale marked in 0.02-inch increments. The pressure drops were estimated to 0.01-inch increments.

V. THEORETICAL AND EXPERIMENTAL RESULTS AND THEIR IMPLICATIONS

A. Velocity Profile

Some theoretical velocity profiles, as predicted from Eq. 32, are plotted to scale in Fig. 10 for the tube geometry $Z_o = 4R_o = 12\delta$ (the geometry of the experimental tube). Profiles for Reynolds numbers of 100, 150, and 200 are plotted at the axial positions $z/Z_o = -1, -0.435, 0, 0.435$, and 1. As shown in Chapter III (Eq. 38) the axial position $z/Z_o = 0.435$ is the incipient separation point for the given geometry, and it was found to occur at a critical Reynolds number of 127.5.

Examination of Eq. 32 reveals that the velocity profiles are composed of a parabolic term plus a term which is multiplied by the slope of the wall. Thus for all Reynolds numbers, the profiles will have a parabolic form at $z/Z_o = -1$, 0, and 1. This form seems reasonable if the wall slope is small, as originally assumed. The profiles at the positions $z/Z_o = -0.435$ and 0.435 are of more interest, so that the following discussion will be limited to these two profiles.

Figure 10a shows the velocity profiles at a Reynolds number of 100. In the converging section the profile has flattened near the center of the tube, while in the diverging section it is nearly parabolic except in the immediate

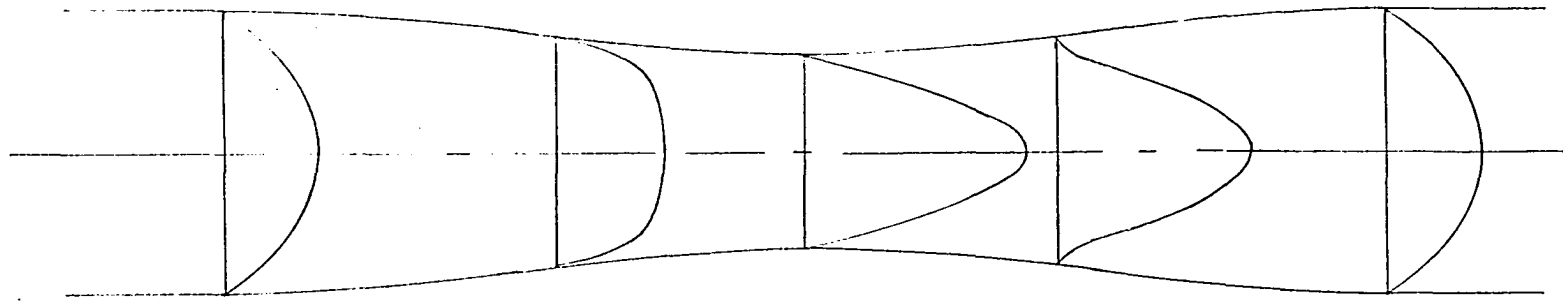

a) $Re_o = 100$

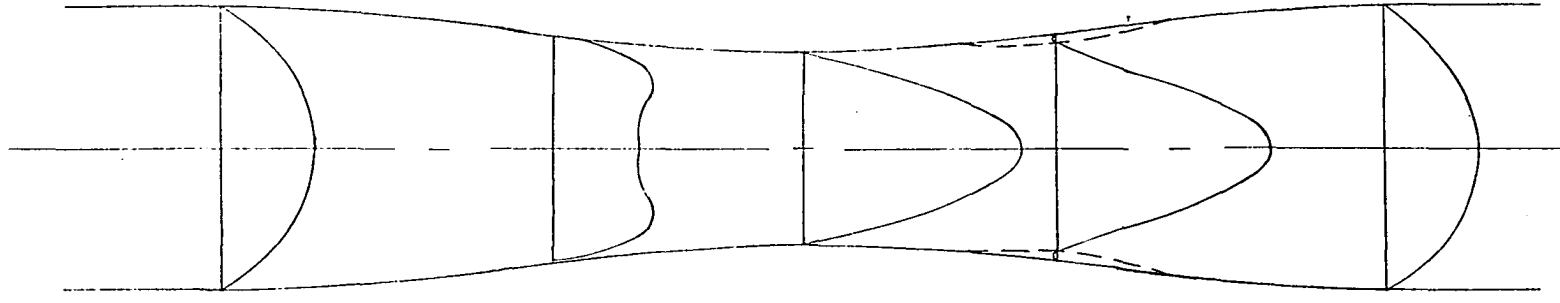

b) $Re_o = 150$

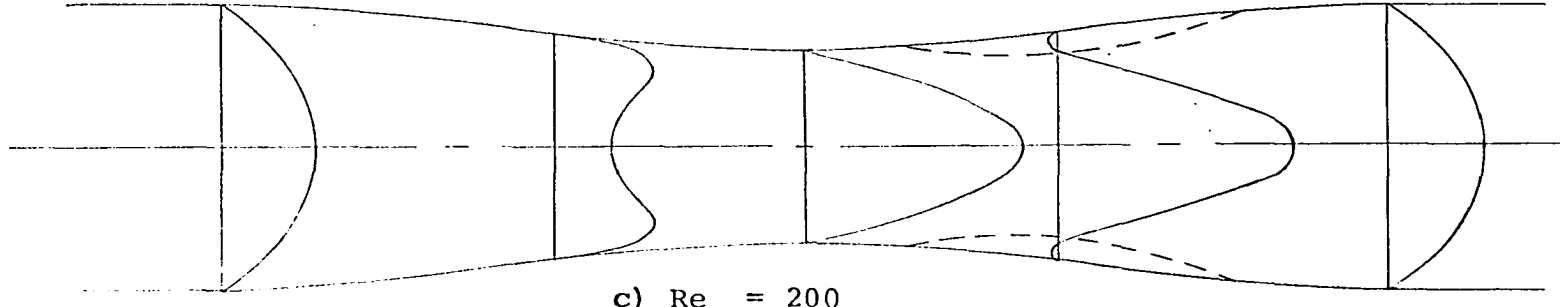

c) $Re_o = 200$

Figure 10. Predicted velocity profiles for the tube geometry $Z_o = 4R_o = 12\delta$

vicinity of the wall. Both of these results seem plausible since the Reynolds number is large enough so that inertia effects cannot be neglected, although still small enough so that separation of the streamlines along the wall does not occur. At a smaller Reynolds number (say 50) both profiles would be more parabolic in form, since the non-parabolic term of Eq. 32 is multiplied by the Reynolds number.

At a Reynolds number of 150 (Fig. 10b) and 200 (Fig. 10c) separation exists in the diverging section. The dotted lines represent the streamlines (or actually the stream surfaces) bounding the separation regions. The locations of these streamlines are determined from Eq. 41. In Fig. 10b they extend from the axial position $z/Z_o = 0.272$ (the separation point) to $z/Z_o = 0.619$ (the reattachment point). In Fig. 10c the separation and reattachment points are at $z/Z_o = 0.182$ and 0.735, respectively. There is circulation of the fluid within the separation region, and Fig. 10c indicates that the thickness of the layer of fluid moving in the downstream direction within the separation region is relatively thin with respect to the layer moving upstream.

Although no attempt was made to determine the velocity profiles in the experimental tube, the profiles shown in the diverging section of the tube (Figs. 10b and 10c) seem quite reasonable. However, the profiles shown in the converging portion at the corresponding section do not have the

form which was expected; that is, it was expected that the higher the Reynolds number became the "flatter" the profile would become. Instead, the theory predicts that for Reynolds numbers greater than the critical Reynolds number required for separation, the maximum axial velocity moves away from the center of the tube. This occurs for axial positions near $z/Z_o = -0.4$ for $Z_o = 4R_o = 12\delta$. At Reynolds numbers of 150 and 200, respectively, the ratios of the maximum velocity to the centerline velocity are 1.12 and 1.53. This ratio increases further as the Reynolds number is increased. Actually, even at the critical Reynolds number, of 127.5, there is a very slight "dip" in the velocity profile near the center of the tube. However, the centerline velocity is within 2% of the maximum velocity.

To the author's knowledge this form of velocity profile has not been either predicted or observed for steady flow in converging geometries. Therefore it is unlikely that such a profile actually exists.

An investigation was made to determine if the dip in the velocity profile occurred near the critical Reynolds (Re_{oc}) number for some other geometries. For $Z_o = 4R_o = 40\delta$, Re_{oc} is 494, and the maximum velocity just begins to move away from the centerline at $Re_o = 490$ (at $z/Z_o = -0.5$). For $Z_o = 4R_o = 8\delta$, Re_{oc} is 73.6. At $Re_o = 70$ the dip is just about to appear at the axial position $z/Z_o = -0.4$. Thus, with respect to the

prediction of the velocity profiles in the converging section of the tube, it appears that the theory is limited to Reynolds numbers up to the critical value to cause separation.

It is not apparent to the author just why the maximum velocity moves away from the centerline of the tube for large Reynolds numbers. However, the last of the conditions listed in Eq. 17 which was used to evaluate the coefficients of the assumed form of the velocity profile (Eq. 16), may provide a partial explanation. In order to obtain the fifth condition given in Eq. 17, use was made of the relation

$$\left(\frac{\partial^2 u}{\partial r^2}\right)_{r=0} = -\frac{2U}{R^2}$$

The assumption was made that at the center of the tube the velocity profile was nearly parabolic; that is

$$u = U\left[1 - \frac{r^2}{R^2}\right]$$

But in the converging section, the inertial effects are expected to "flatten out" the parabolic profile, so that $\left(\frac{\partial^2 u}{\partial r^2}\right)_{r=0}$ is expected to become smaller as the Reynolds number is increased. If this is to happen, the centerline velocity U must be decreased, maybe to such a value that the velocity must increase away from the centerline in order to satisfy the conservation of mass relationship.

Perhaps a better expression for Eq. 17e would be

$$\left(\frac{\partial^2 u}{\partial r^2}\right)_{r=0} = -\frac{4\bar{U}}{R^2}$$

since $U = 2\bar{U}$ for parabolic flow. Then the profile near the center would be forced to be parabolic and have derivatives equal to those obtained for a parabolic profile at the same flow rate. However, away from the centerline the profile is expected to become flat and not have as large a dip in it as calculated by the present analysis.

The velocity profile along the tube determines the values of the wall shearing stress and the separation and reattachment points. A discussion of the implications of these flow characteristics to occlusive vascular disease is given in Sec. E of this chapter.

B. Wall Shearing Stress

The dimensionless form of the wall shearing stress is given by Eq. 34 of Chapter III, and is plotted against the axial position along the stenosis in Fig. 11 for the tube geometry $Z_o = 4R_o = 12\delta$. One immediately observes from Fig. 11 that the shear stress reverses direction (becomes positive) between the points $z/Z_o = 0.185$ and 0.735 and $z/Z_o = 0.085$ and 0.875 for Reynolds numbers of 200 and 400 respectively. These positions represent the separation and reattachment points. Separation does not occur at a Reynolds number of 100; so that along the entire length of the constriction the fluid near the wall is moving in the same direction as the overall flow. It must be remembered that

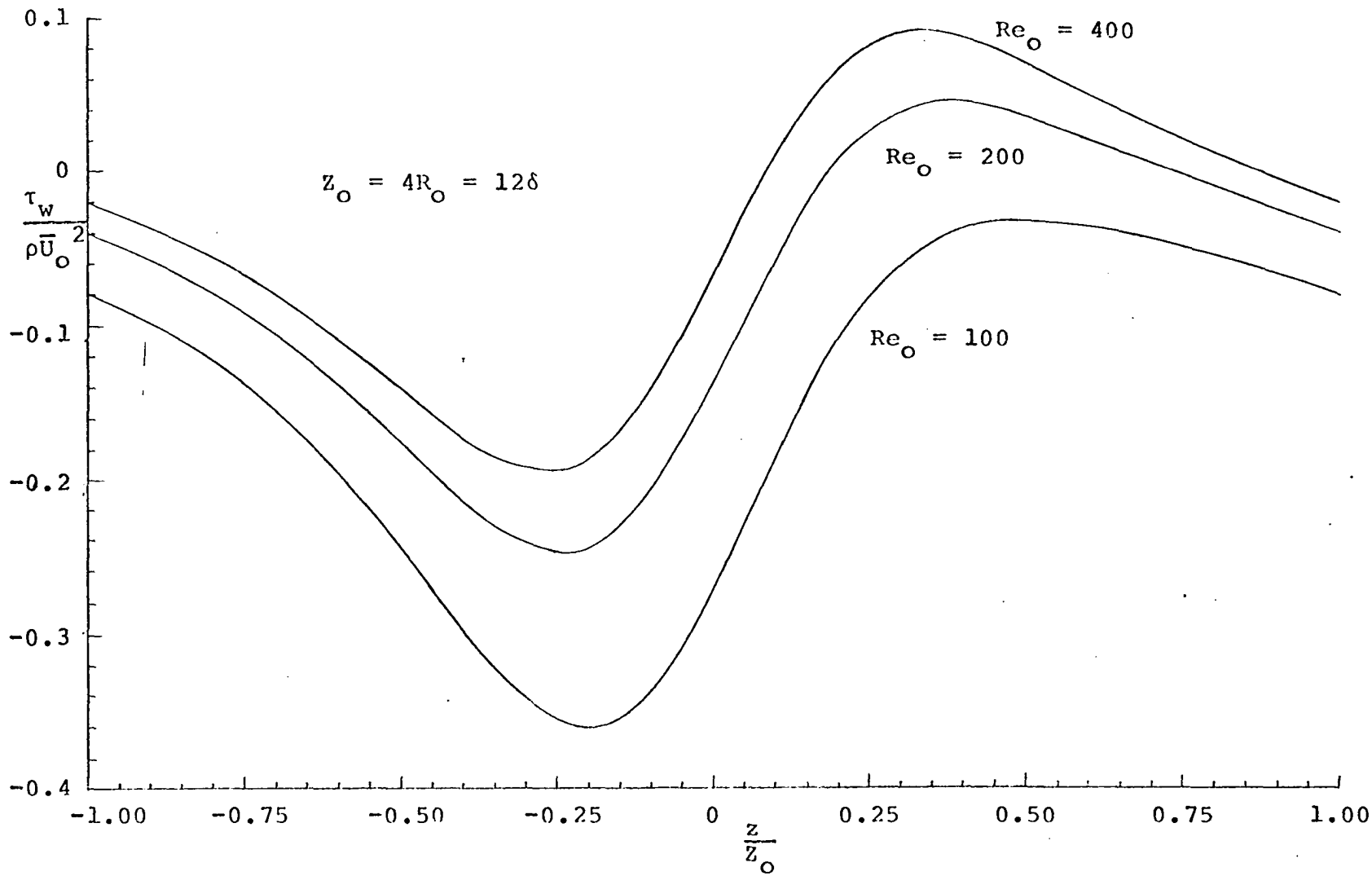

Figure 11. Variation of wall shearing stress along the stenosis

the curves are drawn from an approximate solution to a set of approximate equations, and, as demonstrated in the previous section, it is hazardous to predict quantitative results for Reynolds numbers above the critical value to cause the initial separation (127.5 for the case being studied). However, it is felt that qualitative results may be obtained from the curves, and they are of interest for this reason.

The last term in the equation for the wall shearing stress (Eq. 34) represents the shearing stress due to a parabolic velocity profile. Thus at the two end points of the stenosis $z/Z_o = -1$ and 1, the shearing stress has the same value it would have if the tube had no constriction in it. Therefore, for each of the three curves plotted in Fig. 11, a comparison can be made between the wall shearing stress which exists anywhere along the stenosis with that value (at either end point) which would exist if the walls of the tube were straight and parallel. From Fig. 11 it is seen that the point of maximum shear stress occurs in the converging portion of the tube, and moves upstream from the throat as the Reynolds number is increased. The results predict that the maximum wall shearing stress is 4.5, 6.2, and 9.6 times that value which would exist if there were no constriction, for Reynolds numbers of 100, 200, and 400, respectively.

C. Separation and Reattachment

For any given tube geometry which satisfies Eq. 1 of Chapter III, the critical Reynolds number required to initiate separation can be calculated by substituting Eq. 37 into Eq. 35. For Reynolds numbers greater than this critical value, two values of z/Z_o will satisfy Eq. 35, which correspond to the separation and reattachment points. The theoretical separation-reattachment curve is plotted in Fig. 12 for the tube geometry $Z_o = 4R_o = 12\delta$. Also plotted are the experimental curves obtained when using distilled water, fresh, heparinized, whole bovine blood, and citrated whole human blood which was approximately three months old.

The method used to obtain the data to plot the experimental curves was to inject dye into the separation region, as discussed in Chapter IV, Sec. B2. The separation point was determined to be the point furthest upstream to which the dye moved. The reattachment points for both samples of blood were determined by injecting dye through taps progressively further from the throat of the constriction, until backflow of the dye along the tube wall did not occur. The position of the reattachment point was estimated between the last tap where backflow occurred and the tap immediately downstream from it, with the estimated value depending on the relative velocities of the dye streams leaving the two taps and moving

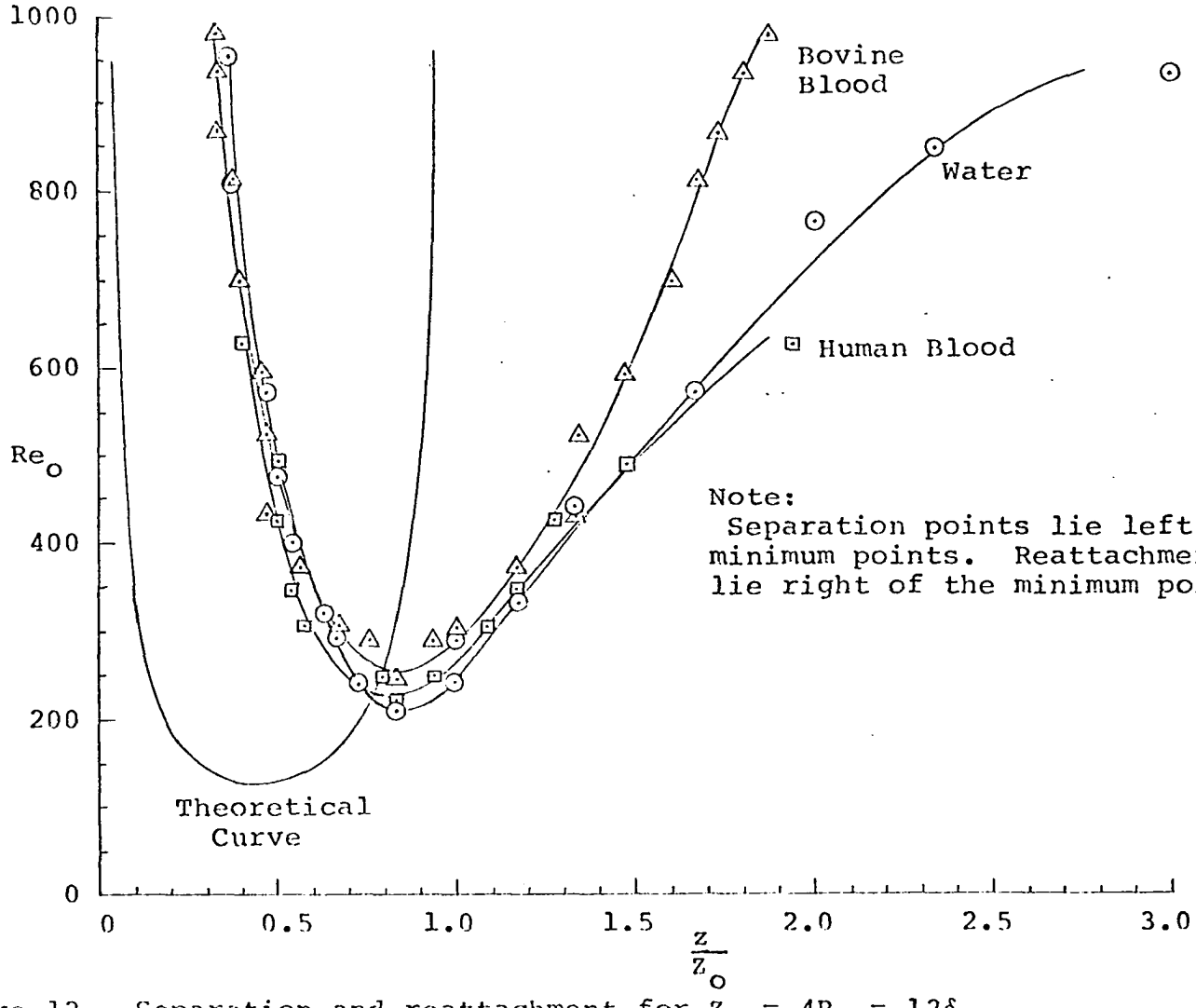

Figure 12. Separation and reattachment for $Z_o = 4R_o = 12\delta$

along the tube wall in opposite directions. When using water in the system, the flow rate was varied until the dye emerging from a wall tap did not flow either upstream or downstream, or, in some cases, it moved in both directions very slowly.

As indicated previously the citrated whole human blood (type O) had a kinematic viscosity of 5.50 centistokes at 24° C, a specific gravity of 1.046, and a hematocrit of 34%. These values did not change while data were being collected. Only five pints of the blood were available. Approximately eight pints of fluid were needed to completely fill the system and provide an overflow from the constant-head tank to the reservoir. Nevertheless, a nearly steady flow of the blood was maintained for flow rates up to 3.1 liters per minute (Re_o = 630) even though the constant-head tank was only partially filled. Higher flow rates were not used as the increased flow rate into the constant-head tank from the Sarns roller pump caused sloshing of the fluid in the partially filled tank. Thus a constant head could not be maintained, and, even more important, there was an excessive amount of foaming of the blood in the tank.

The bovine blood which was run through the system had a kinematic viscosity of 5.73 centistokes at 24° C., a specific gravity of 1.054, and a hematocrit of 43%. These values did not change during the course of the experiment. Sodium heparin (150 mg.) was added to approximately 6 liters of the blood at

the time of collection. The total volume of blood came from one animal, and it was used in the experiments on the same day as it was collected.

A sufficient quantity of bovine blood was available to completely fill the system, so that an overflow from the constant-head tank back to the reservoir could be maintained. Two stainless steel sponges, which had been treated with Antifoam A[1] to retard the formation of foam, were placed in the constant-head tank. However, some foaming of the blood did occur at the higher flow rates. The small bubbles tended to collect at the top of the separation region in the plastic tube, as seen in Fig. 6 of Chapter IV. Most of the bubbles could be moved on downstream by periodically elevating the downstream portion of the tube. However, the presence of a very thin layer of foam at the top of the tube did not appear to affect the results obtained for the separation and reattachment points.

The experimental curves for water, bovine blood, and human blood in Fig. 12 agree very well except for the reattachment points for the bovine blood at Reynolds numbers greater than 450. If the human blood had been fresh, it is possible that it would have behaved somewhat differently. The critical Reynolds number to produce incipient separation

---

[1]Dow Corning Corp., Midland, Michigan.

lies in the range of 200 to 250 for the three fluids studied, as compared to the predicted value of 127.5. Also, the axial position at which separation occurred was approximately at $z/Z_o = 0.85$ as compared to the predicted value of 0.435.

Several possible explanations may be given for the apparent discrepencies between the theoretical and experimental curves. In the order of magnitude analysis given in Chapter III, it was determined that δ/Z_o and δ/R_o should be very small ($<< 1$) in order to obtain Eqs. 9-12. For the converging-diverging tube studied experimentally, $\delta/Z_o = 1/12$ and $\delta/R_o = 1/3$. The reduction of either or both of these ratios could very likely produce experimental results which would agree more closely with those from the theoretical predictions. However, the relative thickness of the separation region would decrease, and thus increase the difficulty of determining experimentally the true end points of the region.

As noted, the tube used in the experiments did not exactly coincide with the geometry expressed by Eq. 1. Also, it was felt that the filament of dye could not be traced entirely back to the actual separation point. At Reynolds numbers near that value to cause incipient separation, even an extremely slow injection of dye into the separation region can result in the dye moving downstream, because it "overshoots" the outer streamline bounding the separation region. Thus, the experimental curves in Fig. 12 may indicate

that the initial separation occurred at a higher critical Reynolds number than was actually the case.

In Fig. 13 a curve is drawn through data points obtained by injecting dye in the converging portion of the tube and following its path in the diverging section with the stereomicroscope. The data points obtained are more scattered when using this method, as it is difficult to estimate just where the dye stream leaves the wall and where it reattaches to the wall, particularly if it does not remain in the same horizontal plane throughout its path. Nevertheless, the limited amount of data collected in this manner indicates that incipient separation may occur at a Reynolds number very near the value of 127.5 that was predicted. However, it must be concluded from all the experimental data that the separation regions were "moved downstream" from the positions predicted theoretically.

It is of interest to look at the variation of the critical Reynolds number and the initial separation point with the variation of the geometry of the constriction. As noted previously, the theory is restricted to constrictions having small slopes, so that Figs. 14 and 15 are intended to only indicate the qualitative nature of these variations. All geometries are assumed to be described by Eq. 1.

Figure 14 predicts how the location of the separation point varies with the parameter δ/R_o. The curve is based on

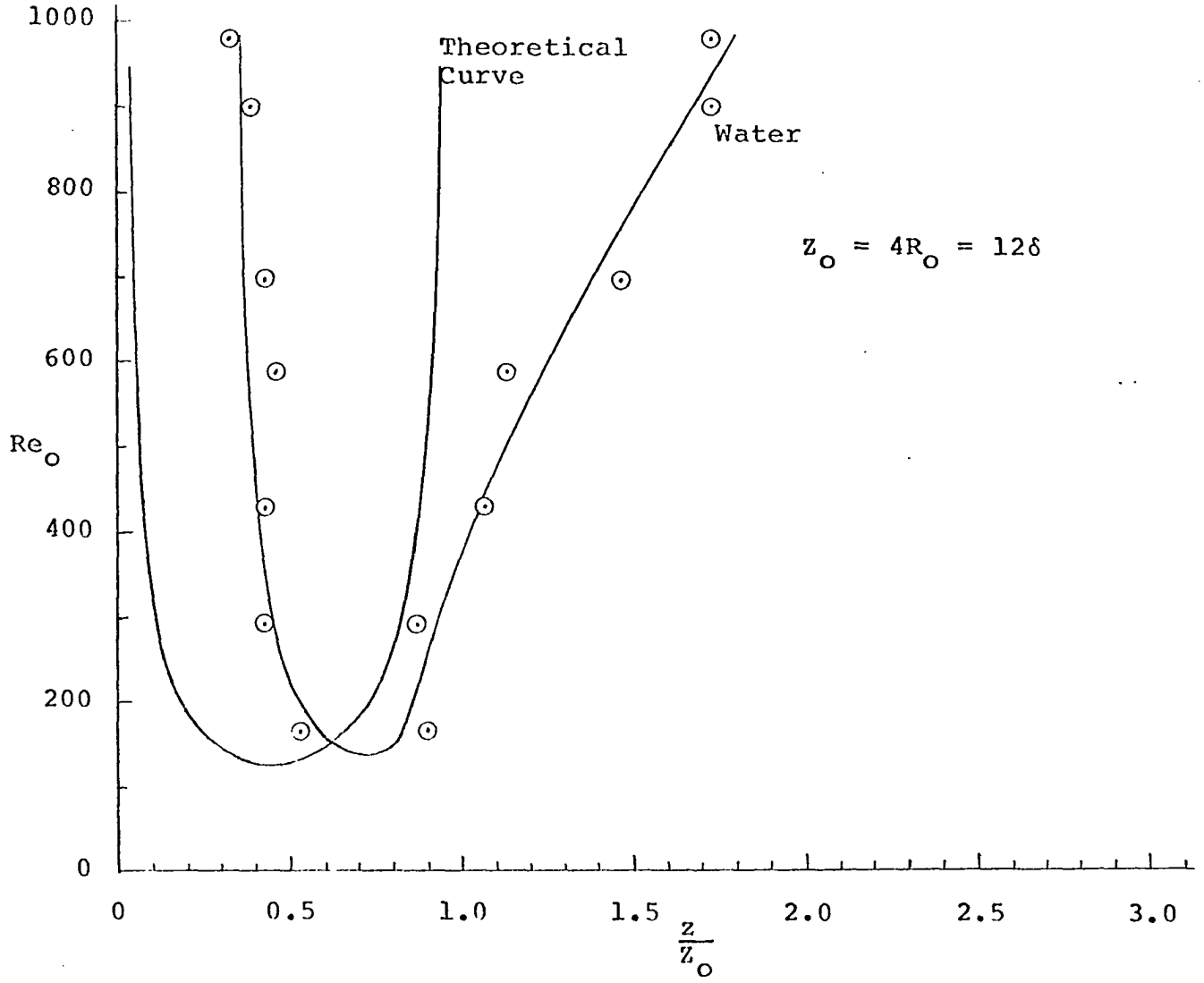

Figure 13. The separation region as determined by injecting dye upstream

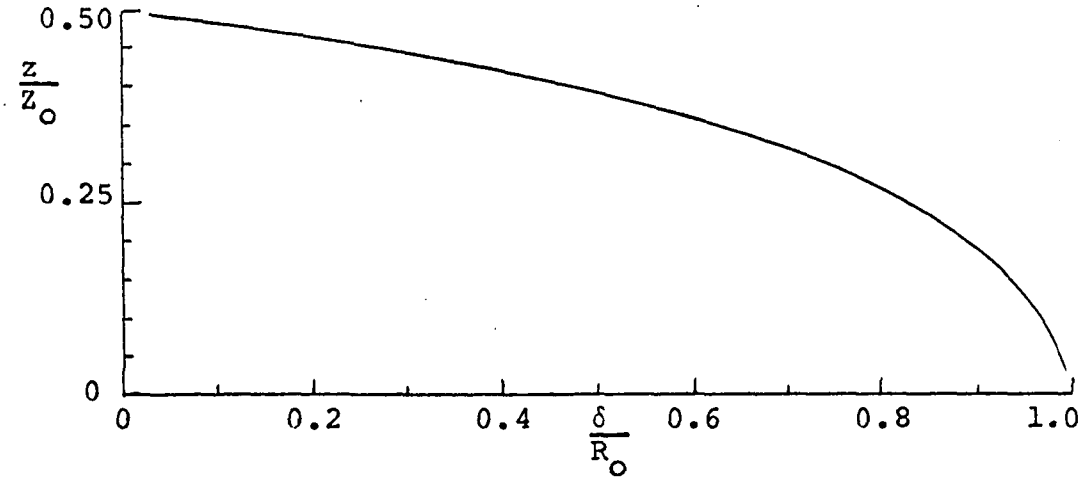

Figure 14. Variation of incipient separation point with height of stenosis

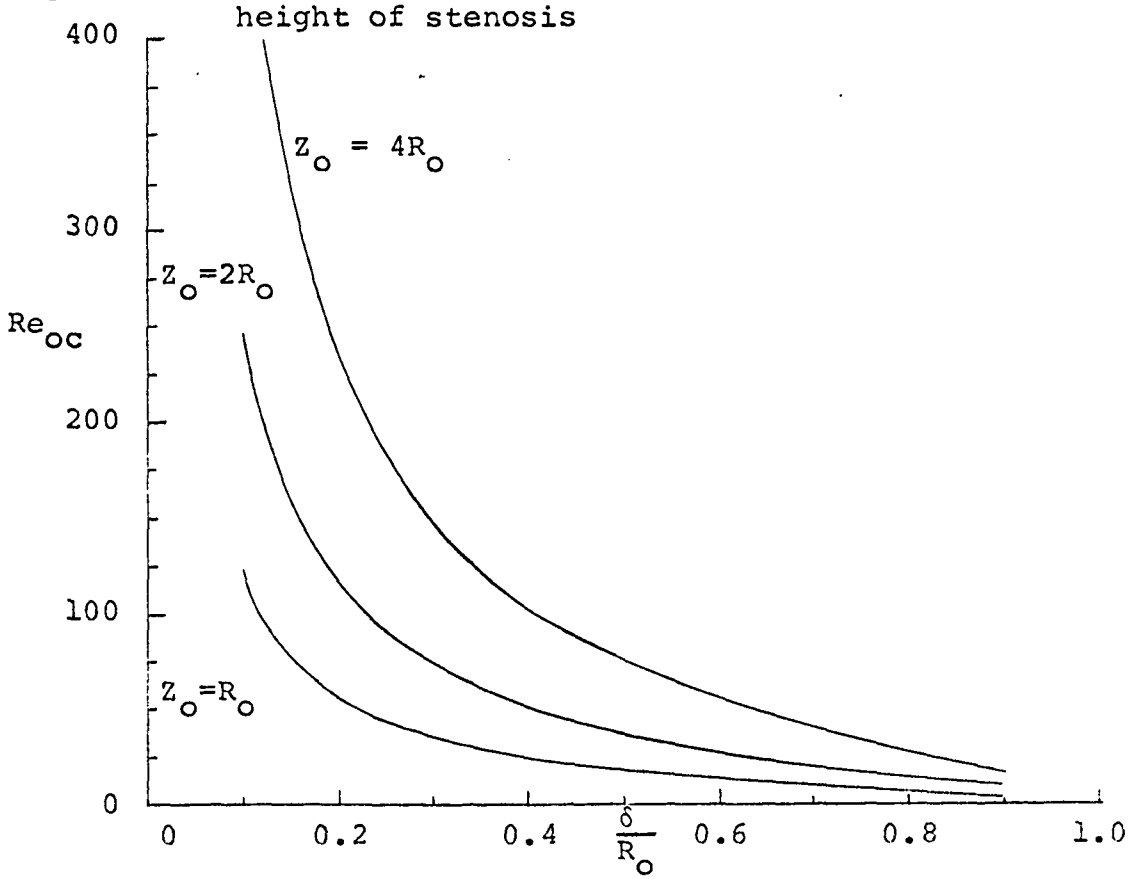

Figure 15. Variation of critical Reynolds number with stenosis height for Z_o/R_o = 1, 2, 4

Eq. 37, and as previously noted this curve does not depend upon the ratio of Z_o/R_o. In Fig. 15 the critical Reynolds number required for incipient separation is plotted against the ratio of the stenosis height to the radius of the straight portion of the tube. As would be expected, the critical Reynolds number is decreased as the slope of the constriction is increased; i.e., as δ/R_o is increased and also as Z_o/R_o is decreased.

D. Pressure Drop

A dimensionless form of the pressure drop from the upstream end of the stenosis ($z = -Z_o$) to any position along the stenosis is given by Eq. 42. Curves drawn from this equation are shown in Fig. 16, for the tube geometry $Z_o = 4R_o = 12\delta$. In order to compare the magnitude of any pressure drop with that value which would be obtained if there were no constriction in the tube, the dotted curves were drawn. These curves represent the dimensionless pressure drops for Poiseuille flow through a straight tube having radius R_o.

It is not intended that quantitative predictions of the pressure drops for Reynolds numbers of 400 and 800 be made. However, the curves are of interest because they indicate how the region of adverse pressure gradient (positive dp/dz) moves toward the throat and toward the end point ($z = Z_o$) as the

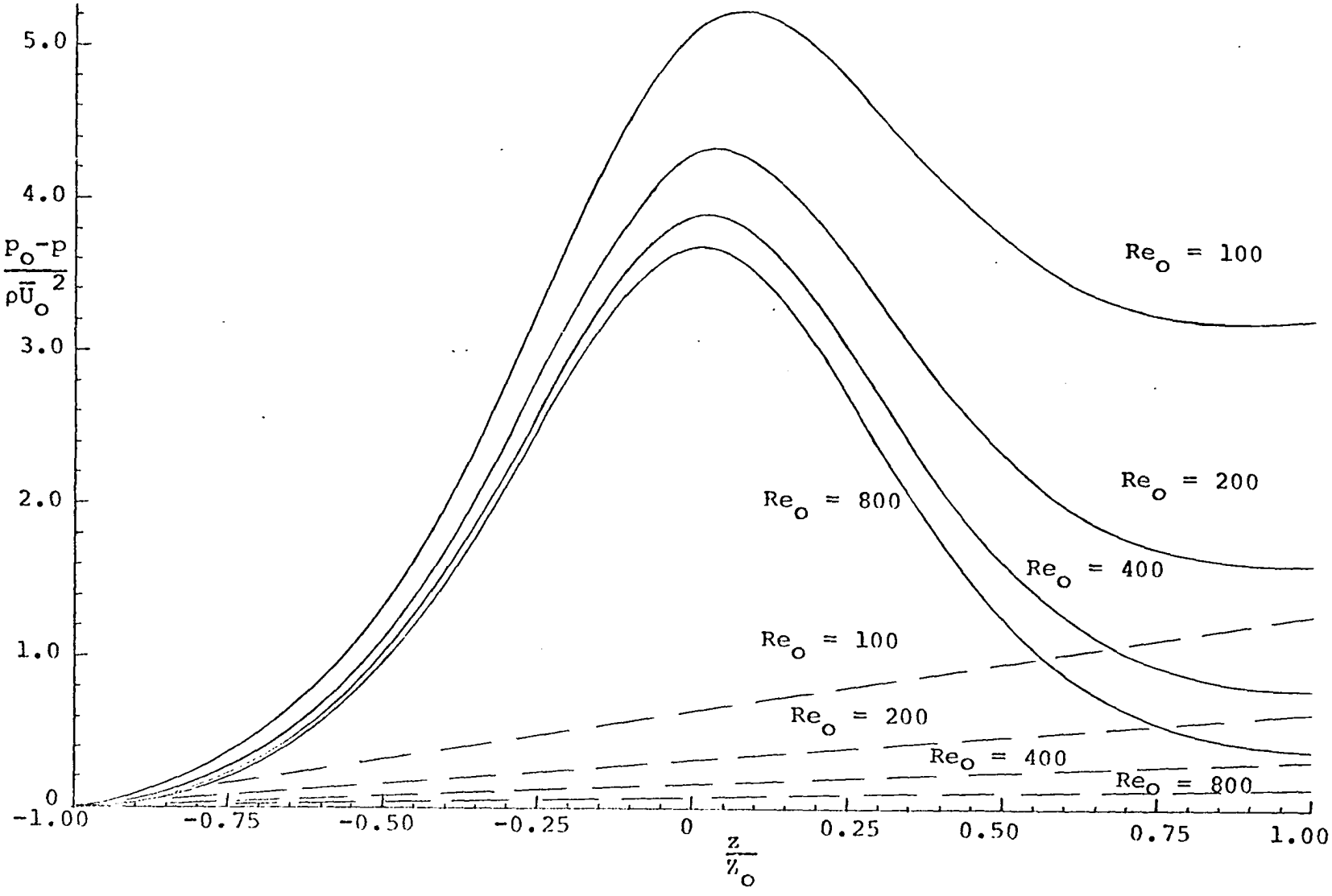

Figure 16. Theoretical pressure drop along the stenosis for $\ell_o = 4R_o = 12\delta$

Reynolds number is increased. It is also interesting to compare the ratio of the maximum pressure drop obtained along the stenosis to that pressure drop which would be obtained if the tube were straight (the dotted curves). At a Reynolds number of 100 this ratio is approximately 7.5. It is seen that the ratio increases as the Reynolds number is increased, whereas the ratio of the pressure drop across the entire stenosis to the pressure drop for the straight tube remains constant (2.5) as the Reynolds number is increased. In actuality this second ratio would also increase with an increasing Reynolds number, but probably not as rapidly as the maximum pressure drop ratio increases.

Pressure drops were measured in the plastic converging-diverging tube from a wall tap 6 inches upstream from the throat of the constriction to a wall tap 6 inches downstream (z/Z_o = -4 to 4). The experimental curves are plotted in Fig. 17. The reason for measuring the pressure drop between the wall taps furthest from the throat was due primarily to the fact that the pressure drops were extremely small. The relatively long length of tubing between the wall taps provided relatively large pressure drops as compared to what would have been obtained across the stenosis. With water flowing through the tube, a pressure drop of only 0.014 inches of water was obtained at a Reynolds number of 1030. The methods of obtaining the experimental data plotted in Fig. 17

Figure 17. Pressure drop from $z = -4Z_o$ to $z = 4Z_o$ for the tube geometry $Z_o = 4R_o = 12\delta$

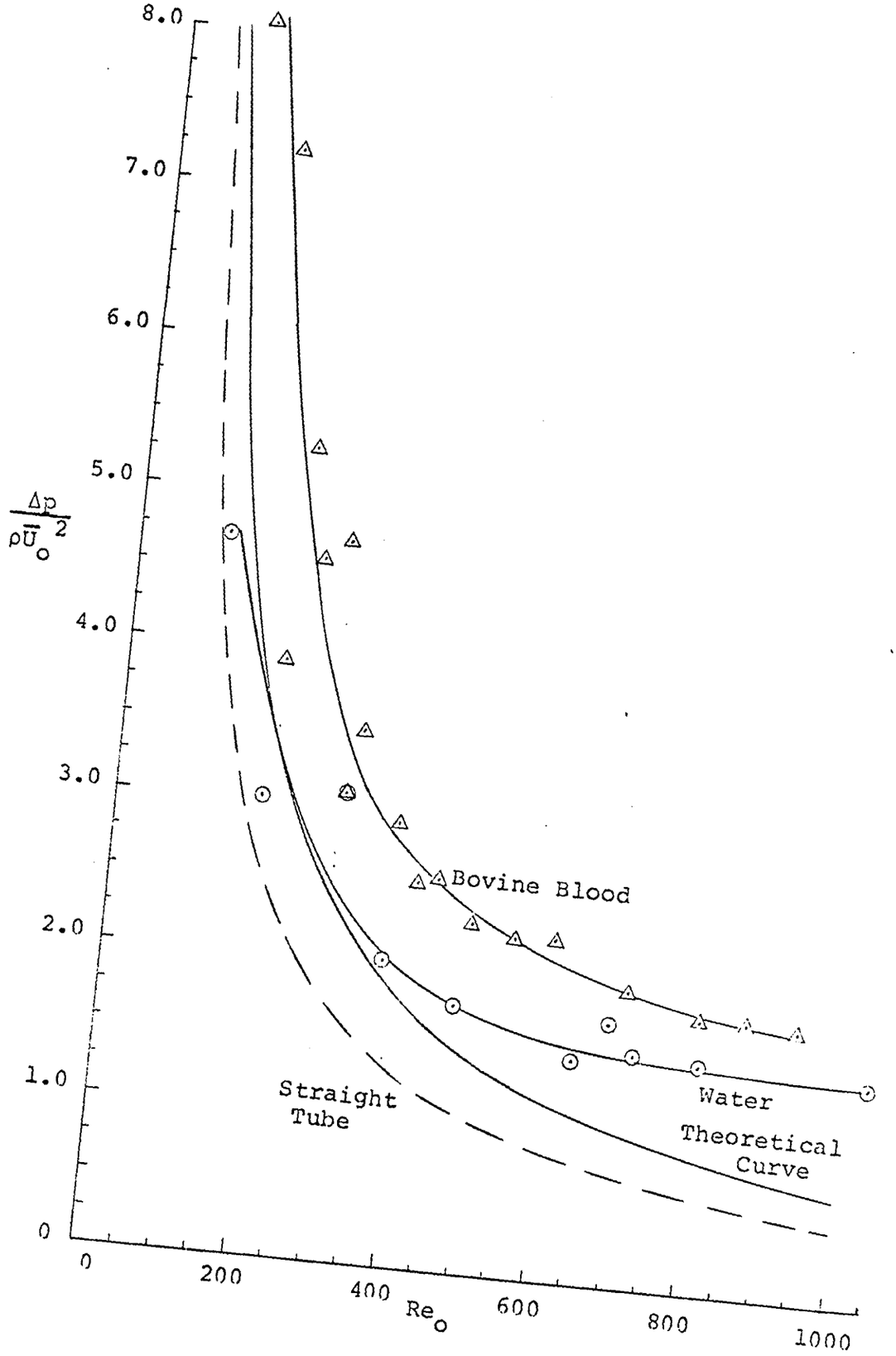
8.0
7.0
6.0
5.0
4.0
3.0
2.0
1.0
0
$\frac{\Delta p}{\rho \bar{U}_o^2}$
0
200
400
600
800
1000
Re_o
Bovine Blood
Water
Straight Tube
Theoretical Curve

are discussed in Sec. B3 of Chapter IV.

The theoretical curve was based on Eq. 44. For any given Reynolds number, the dimensionless pressure drop across the constriction was calculated from Eq. 44, and to this value was added the Poiseuille pressure drop (in dimensionless form) through a straight section of 0.75-inch diameter tubing 9 inches long (since $2Z_o$ = 3 inches is the length of the stenosis). The dotted curve represents the pressure drops which would occur if the tube had no constriction in it (Poiseuille flow over the entire 12-inch length).

With water flowing through the converging-diverging tube, it appears that the theoretical pressure drop curve will predict the actual pressure drop with an error of less than 10% for Reynolds numbers up to 400. Beyond this value the experimental pressure drops are larger than predicted, as is expected since the separation region extends beyond the point $z = Z_o$.

The pressure drops obtained when running bovine blood through the system were larger than the predicted values over the entire range of Reynolds numbers at which pressure drops could be measured (116 to 937). Referring to Fig. 17, it is seen that the experimental curve indicates pressure drops approximately 1.5 times those predicted theoretically for Reynolds numbers up to 400. The ratio increases to

approximately 2 at Reynolds numbers greater than 700. It is not known why such large discrepancies exist between the experimental data for bovine blood and that for water. It is possible that non-Newtonian behavior of the blood causes the dimensionless pressure drops to be higher than for the water. Since blood apparently has a yield stress (13, 14, 15), wall shearing stresses larger than those obtained when using water are likely to exist along the tube near the separation region. In regions of low shearing strain rates (such as near the separation region) the apparent viscosity of the blood is expected to be larger than its value as determined using the capillary tube viscometer. This characteristic of blood might tend to increase the pressure drop. Also, it is observed that for Reynolds numbers greater than approximately 400, the ratio of the dimensionless pressure drop obtained with bovine blood to the dimensionless pressure drop obtained with water begins to decrease from a value of 1.4 to a value of approximately 1.2. If data could have been taken at even larger Reynolds numbers, this ratio may have approached 1.0. A plausible explanation for this phenomenon is that, for the larger Reynolds numbers, the separation region is not as clearly defined as for the smaller values, and larger shearing strain rates exist in and near the separation region; thus the overall behavior of the blood approaches that of a Newtonian fluid as the

Reynolds number is increased.

E. Implication in Occlusive Vascular Disease

Several researchers have suggested that post-stenotic dilatation may be due to turbulence and/or high shearing stresses generated downstream from a stenosis (see for example references 1 and 2). If the constriction is severe so that true turbulence is generated, then it is quite likely that the fluctuating stress (due to fluctuating pressures and velocity gradients) on the endothelial lining causes a deterioration of the endothelial cells, as envisioned by Fry (32). This could lead to the development of atheroma and/or a subsequent degeneration and weaking of the arterial wall. Also, the entire arterial wall may be affected by the high frequency fluctuation of the wall stress and tend to dilate due to autoregulatory mechanisms. It is also possible that in cases where there is a fairly well-defined laminar separation region downstream from a stenosis, deterioration and weakening of the arterial wall may occur due to an insufficient supply of nutrients and oxygen to the arterial wall. This would be due to a relatively small amount of interchange of fluid between the separation region and the main stream of flow.

It is not believed that the increase in average pressure in the diverging portion of a stenosis, as has been suggested

by some investigators, is the cause of post-stenotic dilatation. Indeed, the pressure must be at a lower level than that upstream. Also, the time-average wall shearing stress is expected to be of smaller magnitude than in the converging portion of the stenosis, so that post-stenotic dilatation due to increased wall shearing stress (time-averaged) is unlikely. The possibility exists, however, that the reversed direction of the wall shearing stresses in a separation region may somehow affect the endothelial lining, and cause the artery to dilate due to either autoregulatory mechanisms or to a weakening of the arterial wall.

Some investigators (35) have suggested that a continued ingrowth of tissue near the throat of a stenosis is due to a "suction" effect. The relatively low pressure which occurs just downstream from the throat (see Fig. 16) may tend to lift up the media. Rodbard (2) has a suggested that low shearing stresses downstream from the throat cause the vessel to constrict, and that over a long period of time the artery becomes reorganized around its new geometry. In view of the theory developed, both of these speculations seem plausible. Holman, et al. (36) have suggested that local arterial wall hypertension may lead directly to the development of atheromatous plaques, or indirectly to their development by suppressing the secretion of lipids which are synthesized in the arterial wall. Thus the abnormal

action of pressure and shearing stress on the arterial wall may contribute to atherosclerosis by causing hypertension in the arterial wall.

The development of intravascular thrombi has been related to both turbulence (6, 9) and to stasis (4, 37). Turbulence has been said to precipitate thrombosis (which leads to atheroma) by damaging both the blood and the arterial wall. However, Fox and Hugh (4) state that intravascular thrombosis is more often associated with areas of stasis, and they envision that within static zones fibrin and platelets interact to form a mesh which can trap lipid particles and lead to a plaque of atheroma. Wesolowski, et al. (37) have observed the progression of intravascular mural thrombi through stages of red fibrin, fatty degeneration, fibrosis, and cartilaginous formation which attracts calcium. Since thrombus formation has been related to areas of stasis involved with both prosthetic heart valves and with arterial grafts, it very likely can be related to areas of stasis associated with separation from an arterial stenosis.

Dintenfass (38) speculates that thrombus formation is due to higher blood viscosity causing increased circulation times of the sedimenting aggregates of red blood cells. This leads to progressive hypoxia of the cells and further sedimentation of them. He states that they could then degenerate and likely contribute to thrombus formation. These ideas

may easily be extended to thrombus formation in or near separation regions, as Dintenfass stated that agglutination of red cells increased (with a resulting increase in the apparent viscosity) at low shear rates.

Since blood does have a yield stress, the blood will cease to flow as the rate of shearing strain becomes very small. This may occur near the separation and reattachment points of a stenosis. Further, since an increased concentration of fibrinogen may occur in the interfacial region between the arterial wall and the blood (32), it is possible that a fibrin network may develop in the stagnant blood near the separation and reattachment points.

Fry (32) states that under normal conditions a molecule such as fibrinogen is competing for water, but its affinity for water is lower than that of other substances in the blood. Therefore it tends to be forced into regions where there are fewer free water molecules by the more "aggresive" hydrophilic substances, e.g., albumin. The fewest free water molecules occur at a free surface, and probably at an interface where water molecules are more tightly bonded together. Thus, he speculates that increased concentration of fibrinogen may occur in interfacial regions. Merrill, et al. (15) have concluded that a "structuring" of blood occurs between red blood cells in the presence of fibrinogen, and without fibrinogen blood is nearly Newtonian and has no

yield stress. Thus if the concentration of fibrinogen is high near the arterial wall, it would seem that "structures" of red blood cells might develop in regions of stagnant or nearly stagnant flow, as speculated above. An intravascular clot is expected to develop if conditions are such that fibrinogen is converted to fibrin.

VI. SUMMARY AND CONCLUSIONS

The steady flow through an axisymmetric converging-diverging tube has been studied both theoretically and experimentally, and some possible implications of the flow to the further development of vascular lesions are discussed. The mathematical model is based on the assumptions that the geometry of the constriction is such that the maximum height of the protuberance (δ) is small with respect to both the radius of the straight tube (R_o) and the half-length of the constriction (Z_o). An approximate solution based on these conditions has been obtained. The velocity profile, pressure drop, wall shearing stress, and location of the separation region (when separation does occur) were determined from this solution. These expressions are expected to be valid over the entire length of the stenosis for Reynolds numbers up to the critical value required for separation, and possibly for slightly larger Reynolds numbers in the diverging portion of the tube.

A plastic converging-diverging tube was constructed to determine the separation and reattachment points and the pressure drop across the entire stenosis when both water and blood were flowing through the tube. The experimental results obtained for the water and blood did not differ greatly. However, they did differ from the theoretical results.

According to the theory, the initial separation was expected to occur at a lower Reynolds number (127.5) and at a position closer to the throat of the constriction (z/Z_o = 0.435) than was observed experimentally (approximately 200 and 0.7, respectively). Three primary reasons may be given for the apparent disagreement:

(a) Although carefully constructed, the geometry of the converging-diverging tube did not precisely agree with that studied theoretically.

(b) The method of determining separation is believed to be conservative, in that separation very likely occurs before the injected dye is seen to move upstream.

(c) The ratios of δ/R_o and δ/Z_o were 0.333 and 0.083, respectively. Smaller values, particularly for δ/R_o would have better satisfied the assumptions made in the theoretical analysis.

It is concluded that separation from relatively mild stenosis in a small artery can occur in a range of Reynolds numbers observed in physiological systems. The relatively stagnant flow in small separation regions may contribute to the continued inward growth of a stenosis and/or to post-stenotic dilatation. For larger Reynolds numbers, or a more severe constriction, the turbulence generated in the downstream portion of the separation region most likely contributes to post-stenotic dilatation, perhaps through the

fluctuation of wall stress.

Pressure drops across the entire stenosis were measured when both water and bovine blood were flowing through the converging-diverging tube. Larger pressure drops (in dimensionless form) were obtained when using the blood than when using the water, particularly at Reynolds numbers less than 400. The reason for the discrepancy between the two experimental curves is unknown. The pressure drops for water appeared to be within 10% of those values predicted theoretically, for Reynolds numbers less than 400. If pressure contributes to post-stenotic dilatation, it is perhaps through a fluctuation, rather than through an increase in the average pressure in the diverging portion of a stenosis.

VII. RECOMMENDATIONS FOR FURTHER STUDY

Improvements could be made in the theoretical analysis as were indicated in Chapters III and V. It was noted that Eq. 17e may tend to diminish the centerline velocity U in the converging portion of the tube, so that a "dip" in the velocity profile is obtained near the center of the tube for the larger Reynolds numbers. Simply changing U to $2\overline{U}$ in Eq. 17e may help to remedy this apparent problem. By taking the expression obtained for the velocity profile and substituting it into the integral in Eq. 14, a new solution (a second approximation) will be obtained, which is expected to be a better solution than the first approximation. Of course this procedure could be performed a third time but the calculations become very tedious.

Another possible method of improving the solution would be to use a higher order polynomial for the assumed form of the radial dependence of the velocity profile. The additional relationships which would be needed to evaluate the coefficients could come from the first or second approximations. Also, Eq. 17e could be replaced by a more reasonable expression, obtained from the first or second approximation. Equation 22 can possibly be integrated numerically.

Further investigations are needed to determine the dimensionless pressure drops at various positions along the

stenosis, and to compare those obtained for Newtonian fluids with those obtained when using blood. It is recommended that a glycerol-water solution (approximately 40% glycerol by volume) be used so that the magnitudes of the actual pressure drops are near those obtained when using blood.

Another converging-diverging tube could be constructed so as to more closely satisfy the theoretical geometry and the assumptions made. The larger the tube constructed, the more accurate the geometry obtained should be. However, a larger quantity of fluid will then be needed to fill the system. If it is desired to study the flow characteristics of blood in the experimental tube, then blood from two or more animals may have to be mixed in order to fill the system.

It would be quite interesting to perform some in vivo studies. A small artery could be either externally banded to form an axisymmetric stenosis, or a plug of desired geometry could be inserted into the artery. Both short and long term studies to determine the effects of stenoses of different geometries should be conducted.

VIII. LITERATURE CITED

1. Roach, M. R. An experimental study of the production and time course of poststenotic dilatation in the femoral and carotid arteries of adult dogs. Circulation Research 13: 537-551. 1963.

2. Rodbard, S. Dynamics of blood flow in stenotic vascular lesions. American Heart Journal 72: 698-704. 1966.

3. Young, D. F. Effect of a time-dependent stenosis on flow through a tube. Journal of Engineering for Industry, American Society of Mechanical Engineers Transactions 90: 248-254. 1968.

4. Fox, J. A. and Hugh, A. E. Localization of atheroma: a theory based on boundary layer separation. British Heart Journal 28: 388-399. 1966.

5. Rokitansky, C. Handbuch der pathologischen Anatomie. Braumuller, Vienna, Austria. 1844. Day, G. E. (transl.). A manual of pathological anatomy. Vol. 4. London, England, Sydenham Society. 1852.

6. Mitchell, J. R. A. and Schwartz, C. J. Arterial disease. Oxford, England, Blackwell Scientific Publications. 1965.

7. Gutstein, W. H., Lazzarine-Robertson, A., Jr., and LaTaillade, J. N. The role of local arterial irritability in the development of arterio-atherosclerosis. American Journal of Pathology 42: 61-71. 1963.

8. Rodbard, S. Deposition of flowborne materials on vessel walls. Circulation Research 11: 664-668. 1962.

9. Wesolowski, S. A., Fries, C. C., and Sawyer, P. N. The production and significance of turbulence in hemic systems. American Society for Artificial Internal Organs Transactions 8: 11-18. 1962.

10. McDonald, D. A. Blood flow in arteries. Baltimore, Maryland, Williams and Wilkins Co. 1960.

11. Mandelbaum, I. and Burns, W. H. Pulsatile and non-pulsatile blood flow. Journal of the American Medical Association 191: 657-660. 1965.

12. Bernstein, E. F., Castaneda, A. R., Blackshear, P. L., and Varco, R. L. Prolonged mechanical circulatory support: analysis of certain physical and physiological considerations. Surgery 57: 103-122. 1965.

13. Merrill, E. W. Rheology in medical engineering-human blood and synovial fluid. Engineering in Medicine and Biology Conference Proceedings 20: tutorial. 1967.

14. Merrill, E. W. and Pelletier, G. A. Viscosity of human blood: transistion from Newtonian to non-Newtonian. Journal of Applied Physiology 23: 178-182. 1967.

15. Merrill, E. W., Gilliland, E. R., Lee, T. S., and Salzman, E. W. Blood rheology: effect of fibrinogen deduced by addition. Circulation Research 13: 437-446. 1966.

16. Prandtl, L. and Tietjens, O. G. Applied hydro-and aeromechanics. New York, N.Y., McGraw-Hill Book Co., Inc. 1934.

17. Schlichting, H. Boundary layer theory. 4th ed. New York, N.Y., McGraw-Hill Book Co., Inc. 1960.

18. Vallentine, H. R. Applied hydrodynamics. London, Butterworth and Co. 1959.

19. Rosenhead, L., editor. Laminar boundary layers. Oxford, England, Clarendon Press. 1963.

20. Goldstein, S. Modern developments in fluid dynamics. Vol. I. New York, N.Y., Oxford University Press. 1938.

21. Goldstein, S. Modern developments in fluid dynamics. Vol. 2. New York, N.Y., Oxford University Press. 1938.

22. Blasius, H. Laminare Stömung in Kanälen wechselnder Breite. Zeitschrift f. Mathematik u. Physik 58: 225-233. 1910.

23. Jeffery, G. B. The two-dimensional steady motion of a viscous fluid. Philosophical Magazine 29: 455-465. 1915.

24. Hamel, G. Spiralförmige Bewegung zäher Flüssigkeiten. Jahresber. d. Dt. Mathematiker-Vereinigung 25: 34-60. 1916.

25. Abramowitz, M. On backflow of a viscous fluid in a diverging channel. Journal of Mathematics and Physics 28: 1-21. 1949.

26. Langlois, W. E. Slow viscous flow. New York, N.Y., Macmillan Co. 1964.

27. Patterson, G. N. Viscosity effects in a channel of small exponential divergence. Canadian Journal of Research 12: 676-685. 1935.

28. Patterson, G. N. Flow forms in a channel of small exponential divergence. Canadian Journal of Research 11: 770-779.

29. Rodbard, S. Physical factors in the progression of stenotic vascular lesions. Circulation 17: 410-417. 1958.

30. Brice, J. G., Dowsett, D. J., and Lowe, R. D. Haemodynamic effects of carotid artery stenosis. British Medical Journal 2: 1363-1366. 1964.

31. Shipley, R. E. and Gregg, D. E. The effect of external constriction of a blood vessel on blood flow. American Journal of Physiology 141: 289-296. 1944.

32. Fry, D. L. Acute vascular endothelial changes associated with increased blood velocity gradients. Circulation Research 22: 165-197. 1968.

33. Kline, S. J. Similitude and approximation theory. New York, N.Y., McGraw-Hill Book Co., Inc. 1965.

34. Barnard, A. C. L., Hunt, W. A., Timlake, W. P., and Varley, E. A theory of fluid flow in compliant tubes. Biophysical Journal 6: 717-724. 1966.

35. Texon, M., Imparato, A. M., Lord, J. W., Jr. The hemodynamic concept of atherosclerosis. American Medical Association Archives of Surgery 80: 47-53. 1960.

36. Holman, R. L., McGill, H. C., Strong, J. P., and Geer, J. C. Filtration versus local formation of lipids in pathogenosis of atherosclerosis. American Medical Association Journal 170: 416-420. 1959.

37. Wesolowski, S. A., Sauvage, L. R., Ping, R. S., and Fries, C. C. Dynamics of blood flow in graft disproportions and in normal blood vessels. Surgical Forum 6: 227-233. 1956.

38. Dintenfass, L. Thixotropy of blood and proneness to thrombus formation. Circulation Research 11: 233-239. 1962.

39. Hodgman, C. D. Standard mathematical tables. Cleveland, Ohio, Chemical Rubber Publishing Co. 1955.

IX. ACKNOWLEDGMENTS

I wish to take this opportunity to express my sincere appreciation to Dr. Donald F. Young for his guidance and encouragement throughout the course of this investigation.

I would like to thank Dr. Young, Dr. H. J. Weiss, and Dr. N. R. Cholvin for their assistance in obtaining fellowships and assistantships, so that full-time study was possible.

Finally, I wish to acknowledge the patience and inspiration of my wife, Jean, and son, Douglas, for without them there would be no joy in accomplishment.

X. APPENDIX A: DEVELOPMENT OF WALL SHEARING STRESS RELATIONSHIP

In order to develop an expression for the wall shearing stress, forces are summed on a small volume of fluid adjacent to the wall in the diverging portion of the tube. Figure 18 shows such an element of fluid, and the forces acting on the element. When the forces acting on the fluid in the radial and axial directions are set equal to zero one obtains, respectively

$$\sigma_w A_1 \cos\theta = \sigma_{rr} A_2 - \tau_{zr} A_3 - \tau_w A_1 \sin\theta + 2\sigma_{\theta\theta} A_4 \sin\frac{\Delta\beta}{2} \qquad \text{(A1)}$$

and

$$\tau_w A_1 \cos\theta = \sigma_w A_1 \sin\theta - \sigma_{zz} A_3 + \tau_{rz} A_2 \qquad \text{(A2)}$$

where the inertia terms have been left out of Eqs. A1 and A2 since they will drop out when ΔR, ΔL, and $\Delta\beta$ are allowed to go to zero.

The stresses and areas as given on Fig. 18 are now substituted into Eq. A2 (where σ_w is substituted from Eq. A1) and the resulting equation is divided by $R\Delta\beta\Delta L$. One obtains:

$$\begin{aligned}\tau_w(1 + \tan^2\theta) &= (p - 2\mu\frac{\partial u}{\partial z})(\tan\theta) \\ &+ \mu(\frac{\partial v}{\partial z} + \frac{\partial u}{\partial r})(1 - \frac{\Delta R}{2R}) + (-p + 2\mu\frac{\partial v}{\partial r})(\tan\theta)(1 - \frac{\Delta R}{2R}) \\ &- \mu(\frac{\partial v}{\partial z} + \frac{\partial u}{\partial r})(\tan^2\theta) + (-p + 2\mu\frac{v}{r})(\frac{\Delta R}{R})(\tan\theta)(\frac{\sin\frac{\Delta\beta}{2}}{\Delta\beta}) \qquad \text{(A3)}\end{aligned}$$

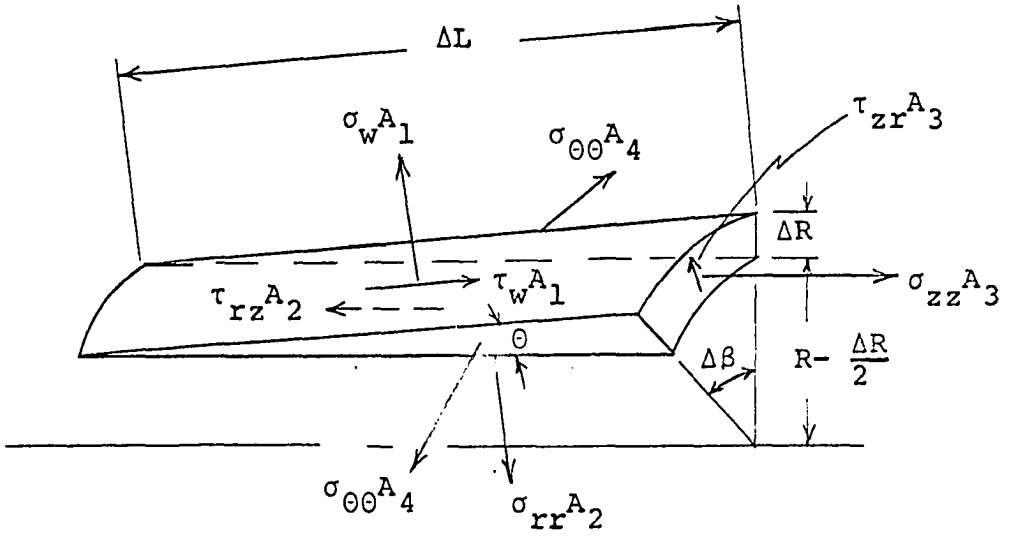

$$\sigma_{rr} = -p + 2\mu \frac{\partial v}{\partial r} \qquad A_1 = R\Delta\beta\Delta L$$

$$\sigma_{\theta\theta} = -p + 2\mu\left(\frac{v}{r}\right) \qquad A_2 = \left(R-\frac{\Delta R}{2}\right)(\Delta\beta)(\Delta L \cos\theta)$$

$$\sigma_{zz} = -p + 2\mu \frac{\partial u}{\partial z} \qquad A_3 = R\Delta\beta(\Delta L \sin\theta)$$

$$\tau_{rz} = \tau_{zr} = \mu\left(\frac{\partial v}{\partial z} + \frac{\partial u}{\partial r}\right) \qquad A_4 = \frac{\Delta R}{2}(\Delta L \cos\theta)$$

Figure 18. Free-body diagram of a fluid element

The incremental volume of fluid is now allowed to shrink to a point (ΔL, ΔR, and $\Delta\beta$ approach zero). Thus the wall shearing stress at any point along the tube is given by

$$\tau_w(\sec^2\Theta) = 2\mu\left(\frac{\partial v}{\partial r} - \frac{\partial u}{\partial z}\right)\tan\Theta + \mu\left(\frac{\partial v}{\partial z} + \frac{\partial u}{\partial r}\right) - \mu\left(\frac{\partial v}{\partial z} + \frac{\partial u}{\partial r}\right)\tan^2\Theta \qquad \text{(A4)}$$

Equation A4 is put into dimensionless form by the transformations given in Eq. 5 of the text.

$$\frac{\tau_w}{\rho\bar{U}_o^2}\sec^2\Theta = \frac{2\nu}{U_o R_o}\left[\frac{\delta}{Z_o}\frac{\partial\bar{v}}{\partial\bar{r}} - \frac{R_o}{Z_o}\frac{\partial\bar{u}}{\partial\bar{z}}\right]\tan\Theta + \frac{\nu}{U_o R_o}\left[\frac{\delta}{Z_o}\frac{R_o}{Z_o}\frac{\partial\bar{v}}{\partial\bar{z}} + \frac{\partial\bar{u}}{\partial\bar{r}}\right][1 - \tan^2\Theta] \qquad \text{(A5)}$$

It was shown by Eq. 8 that $\frac{\partial\bar{u}}{\partial\bar{z}} \sim 0\left(\frac{\delta}{R_o}\right)$. Also, since the angle Θ must be small, $\sec\Theta$ and $\tan\Theta$ may be approximated by 1 and 0, respectively. Since $\frac{\delta}{Z_o} = \varepsilon << 1$, and $R_o \sim 0(Z_o)$, all terms on the right hand side are negligibly small as compared to $\frac{\nu}{U_o R_o}\frac{\partial\bar{u}}{\partial\bar{r}}$. Thus, the wall shearing stress can be approximated by

$$\tau_w = \mu\left(\frac{\partial u}{\partial r}\right) \qquad \text{(A6)}$$

where the derivative is evaluated at r=R.

XI. APPENDIX B: DEVELOPMENT OF PRESSURE DROP RELATIONSHIP

It is desired to integrate Eq. 28 using the conditions that $p = p_o$ and $R = R_o$ at $z = -Z_o$. Thus

$$\int_{p_o}^{p} dp = \frac{5432}{1575\Pi^2} \rho Q^2 \int_{R_o}^{R} \frac{1}{R^5} dR - \frac{8\mu Q}{\Pi} \int_{-Z_o}^{z} R^{-4} dz \tag{B1}$$

or

$$p - p_o = \frac{5432}{1575\Pi^2} \rho Q^2 \left[-\frac{1}{4} R^{-4}\right]_{R_o}^{R} - \frac{8\mu Q}{\Pi} \int_{-Z_o}^{z} \frac{dz}{R^4}$$

Substituting in $R = R_o - \frac{\delta}{2}\left(1 + \cos \frac{\Pi z}{Z_o}\right)$ one obtains

$$p - p_o = -\frac{1358}{1575\Pi^2} \rho Q^2 \left\{\frac{1}{\left[R_o - \frac{\delta}{2}\left(1 + \cos \frac{\Pi z}{Z_o}\right)\right]^4} - \frac{1}{R_o^4}\right\}$$

$$- \frac{8\mu Q}{\Pi} \int_{-Z_o}^{z} \frac{dz}{\left[R_o - \frac{\delta}{2}\left(1 + \cos \frac{\Pi z}{Z_o}\right)\right]^4} \tag{B2}$$

Since both the bracketed term and the integral in the above expression are positive, $p - p_o$ will be negative all along the stenosis, as, of course, must be the case. In dimensionless form, Eq. B2 becomes

$$\frac{p - p_o}{\rho \bar{U}_o^2} = -\frac{1358}{1575} R_o^4 \left\{\frac{1}{\left[R_o - \frac{\delta}{2}\left(1 + \cos \frac{\Pi z}{Z_o}\right)\right]^4} - \frac{1}{R_o^4}\right\}$$

$$- 16 \frac{R_o^3}{Re_o} \int_{-Z_o}^{z} \frac{dz}{\left[R_o - \frac{\delta}{2}\left(1 + \cos \frac{\Pi z}{Z_o}\right)\right]^4} \tag{B3}$$

where $Re_o = \frac{2\bar{U}_o R_o}{\nu}$. The integral in B3 is evaluated as follows:

Let

$$I = \int_{-Z_o}^{z} \frac{dz}{[R_o - \frac{\delta}{2}(1 + \cos \frac{\Pi z}{Z_o})]^4} = \frac{Z_o}{\Pi} \int_{-\Pi}^{\frac{\Pi z}{Z_o}} \frac{d\theta}{(a+b\cos\theta)^4} \quad (B4)$$

where

$$a = R_o - \frac{\delta}{2} \qquad b = -\frac{\delta}{2} \qquad \theta = \frac{\Pi z}{Z_o} \quad (B5)$$

Let

$$x = \tan \frac{\theta}{2} = \tan \frac{\Pi z}{2Z_o} \quad (B6)$$

Then

$$\cos\theta = 1-(1-\cos\theta) = 1-2\sin^2\frac{\theta}{2} = (1-\sin^2\frac{\theta}{2}) - \sin^2\frac{\theta}{2}$$

$$= \frac{\cos^2\frac{\theta}{2} - \sin^2(\frac{\theta}{2})}{\cos^2\frac{\theta}{2} + \sin^2(\frac{\theta}{2})} = \frac{1-\tan^2(\frac{\theta}{2})}{1+\tan^2(\frac{\theta}{2})} = \frac{1-x^2}{1+x^2}$$

and

$$d\theta = 2(\cos^2\frac{\theta}{2})dx = \frac{2}{1+x^2}\,dx$$

Therefore

$$I = \frac{2Z_o}{\Pi} \int_{\tan(\frac{-\Pi}{2})}^{\tan\frac{\Pi z}{2Z_o}} [\frac{1}{1+x^2}] [\frac{1}{a+b[\frac{1-x^2}{1+x^2}]}]^4 \, dx$$

$$= \frac{2Z_o}{\Pi} \int_{\tan(\frac{-\Pi}{2})}^{\tan\frac{\Pi z}{2Z_o}} \frac{(1+x^2)^3}{[(a+b) + x^2(a-b)]^4} \, dx$$

$$= \frac{2Z_o}{\Pi(a-b)^4} \int_{\tan(\frac{-\Pi}{2})}^{\tan\frac{\Pi z}{2Z_o}} \frac{(1+x^2)^3}{(c+x^2)^4}\, dx = \frac{2Z_o}{\Pi R_o^4} \int_{\tan(\frac{-\Pi}{2})}^{\tan\frac{\Pi z}{2Z_o}} \frac{(1+x^2)^3}{(c+x^2)^4}\, dx \tag{B7}$$

where

$$c = \frac{a+b}{a-b} = \frac{R_o - \frac{\delta}{2} - \frac{\delta}{2}}{R_o - \frac{\delta}{2} + \frac{\delta}{2}} = \frac{R_o - \delta}{R_o} \tag{B8}$$

The function inside the integral in Eq. B7 is now expanded into partial fractions

$$\frac{(1+x^2)^3}{(c+x^2)^4} = \frac{A}{c+x^2} + \frac{B}{(c+x^2)^2} + \frac{D}{(c+x^2)^3} + \frac{E}{(c+x^2)^4}$$

Solving for A, B, D, and E and substituting into Eq. B7 gives

$$I = \frac{2Z_o}{\Pi R_o^4} \{\int \frac{dx}{c+x^2} + 3(1-c)\int \frac{dx}{(c+x^2)} + 3(1-c)^2 \int \frac{dx}{(c+x^2)^3}$$

$$+ (1-c)^3 \int \frac{dx}{(c+x^2)^4}\}_{x=\lim_{z\to -Z_o}}^{x=\tan\frac{\Pi z}{2Z_o}} [\tan\tfrac{\Pi z}{2Z_o}] \tag{B9}$$

where the superscript and subscript on the last bracket denote that all integrals are evaluated at these limits. The four integrals are evaluated using standard tables (39) and Eq. B9 becomes

$$I = \frac{2Z_o}{\Pi R_o^4} \{\frac{1}{\sqrt{c}} \arctan \frac{x}{\sqrt{c}} + 3(1-c)[\frac{x}{2c(c+x^2)} + \frac{1}{2c\sqrt{c}} \arctan \frac{x}{\sqrt{c}}]$$

$$+\frac{3(1-c)^2}{4c}\left[\frac{x}{(c+x^2)^2}+\frac{3x}{2c(c+x^2)}+\frac{3}{2c\sqrt{c}}\arctan\frac{x}{\sqrt{c}}\right]$$

$$+\frac{(1-c)^3}{6c}\left[\frac{x}{(c+x^2)^3}+\frac{5x}{4c(c+x^2)^2}+\frac{15x}{8c^2(c+x^2)}+\frac{15}{8c^2\sqrt{c}}\arctan\frac{x}{\sqrt{c}}\right]$$

$$+\frac{\Pi}{2}\left[\frac{1}{\sqrt{c}}+\frac{3(1-c)}{2c\sqrt{c}}+\frac{9(1-c)^2}{8c^2\sqrt{2}}+\frac{5(1-c)^3}{16c^3\sqrt{c}}\right]\Bigg\} \qquad \text{(B10)}$$

where x and c are given by Eqs. B6 and B8. When Eq. A10 is substituted into B3, the pressure drop from $z = -Z_o$ to the desired cross section along the stenosis is obtained.

Of particular interest is the total pressure drop across the stenosis. This is obtained by letting $z \to Z_o$ in Eq. B3 (after first substituting Eq. B10 into Eq. B3. Thus

$$\left(\frac{p-p_o}{\rho\bar{U}_o^2}\right)_T = -\frac{32}{Re_o}\frac{Z_o}{R_o}\left[\frac{1}{\sqrt{c}}+\frac{3(1-c)}{2c\sqrt{c}}+\frac{9(1-c)^2}{8c^2\sqrt{c}}+\frac{5(1-c)^3}{16c^3\sqrt{c}}\right] \qquad \text{(B11)}$$

where the subscript T denotes the total pressure drop and

$$c = 1-\frac{\delta}{R_o}$$

It is noted that Equation B4 for I can be evaluated by the theory of residues when the upper limit is Z_o. This was carried out and the result checked with Eq. B11.

XII. APPENDIX C: TABULATED DATA

Table 1. Original test data

Fluid	Temperature (°C)	Specific Gravity	Viscosity (centistokes)	Hematocrit (%)	Flow Rate (ml/sec)	Separation Point (z, in.)	Reattachment Point (z, in.)	Pressure Drop (in. of fluid)
water	26.0	1.000	0.875	-	2.8	1.25	-	-
					3.1	1.10	1.50	
					3.8	1.00	1.50	
					4.2	0.95	-	
					4.4	-	1.75	
					5.3	0.82	-	
					5.8	-	2.00	
					6.3	0.75	-	
					7.5	0.70	2.5	
					10.0	-	3.0	
					10.6	0.55	-	
					11.1	-	3.5	
					12.2	-	4.5	
					12.5	0.55	-	
water	24.6	1.000	0.902	-	13.9	-	-	0.0140
					10.9			0.0090
					9.6			0.0070
	24.8		0.897		9.1			0.0071
					8.5			0.0052
					6.4			0.0035
					5.0			0.0027
					4.1			0.0025
					2.6			0.0010
					1.6			0.0006
					0			0

Table 1 (Continued)

Fluid	Temp. erature (°C)	Specific Gravity	Viscosity (centi-stokes)	Hematocrit (%)	Flow Rate (ml/sec)	Separa-tion Point (z, in.)	Reattach-ment Point (z, in.)	Pressure Drop (in. of fluid)
bovine blood	24.0	1.054	5.73	43	21.0	1.25	1.25	-
					24.8	1.15	1.40	
					26.2	1.00	1.50	
					32.3	0.85	1.75	
					37.1	0.70	2.0	
					45.0	0.70	2.0	
					51.0	0.68	2.2	
					60.0	0.60	2.4	
					70.0	0.55	2.5	
					74.5	0.50	2.6	
					80.5	0.50	2.7	
					84.0	0.49	2.8	
					10.0	-	-	0.04
					17.6			0.06
					25.8			0.10
					51.5			0.29
					60.0			0.35
					68.5			0.42
					73.7			0.49
					79.5			0.56
					23.5			0.13
					19.5			0.10
					14.0			0.07
					21.0			0.10
					27.5			0.13
					32.5			0.15
					35.5			0.16
					37.5			0.18
					42.0			0.20
					47.5			0.25

Table 1 (Continued)

Fluid	Temperature (°C)	Specific Gravity	Viscosity (centistokes)	Hematocrit (%)	Flow Rate (ml/sec)	Separation Point (z, in.)	Reattachment Point (z, in.)	Pressure Drop. (in. of fluid)
human blood	24.0	1.046	5.50	32	18.0	1.25	1.25	-
					20.6	1.20	1.40	
					25.0	0.85	1.62	
					28.5	0.80	1.75	
					35.0	0.75	1.90	
					40.6	0.75	2.2	
					52.0	0.60	2.9	
water	26.0	1.000	0.875		2.2	0.80	1.30	
	26.0		0.875		3.9	0.65	1.35	
	25.0		0.893		5.8	0.65	1.60	
	25.0		0.893		13.1	0.50	2.60	
	26.0		0.875		7.7	0.70	1.70	
	26.0		0.875		9.1	0.65	2.20	
	26.0		0.875		11.8	0.58	2.60	